

SINGLE-COLUMN MODEL SIMULATIONS
OF ARCTIC CLOUDINESS AND SURFACE RADIATIVE FLUXES
DURING THE SURFACE HEAT BUDGET OF ARCTIC (SHEBA) EXPERIMENT

By

Cécile Hannay

RECOMMENDED:

Advisory Committee Chair

Department Head

APPROVED:

Dean, (College of Science, Engineering and Mathematics)

Dean of the Graduate School

Date

SINGLE-COLUMN MODEL SIMULATIONS
OF ARCTIC CLOUDINESS AND SURFACE RADIATIVE FLUXES
DURING THE SURFACE HEAT BUDGET OF ARCTIC (SHEBA) EXPERIMENT

A
THESIS

Presented to the Faculty
of the University of Alaska Fairbanks
in Partial Fulfillment of the Requirements
for the Degree of

MASTER IN ATMOSPHERIC SCIENCES

By
Cécile Hannay, Licenciée en Sciences Physiques

Fairbanks, Alaska

August 2001

Abstract

We evaluate the ability of a typical cloud parameterization from a global model (CCM3 from NCAR) to simulate the Arctic cloudiness and longwave radiative fluxes during wintertime. Simulations are conducted with a Single-Column Model (SCM) forced with observations and reanalysis data from the Surface Heat Budget of the Arctic Ocean (SHEBA) experiment. Typically, the SCM overestimates the Arctic cloud fraction and the downwelling longwave flux. Moreover, the SCM does not capture accurately the temperature and moisture profiles, and the surface flux fields. Relaxing temperature and moisture profiles to observed values dramatically improves the simulations. This suggests that the cloud parameterization of CCM3 is suitable for Arctic clouds, as long as the temperature and moisture fields are captured correctly. Sensitivity studies show that the cloud fraction is not very sensitive to cloud type, ice effective radius, ice liquid ratio amount and uncertainty of the advective forcing.

Table of contents

List of figures.....	6
List of tables.....	8
Acknowledgments.....	9
CHAPTER 1 - INTRODUCTION.....	10
1. 1. Cloud impacts on the radiative budget	10
1. 2. Arctic cloudiness characteristics	13
1.2.1 Observed climatologies of Arctic cloudiness	13
1.2.2 Prediction of Arctic cloud cover by GCMs.....	15
CHAPTER 2 - MODEL DESCRIPTION	17
2. 1. Single-Column model: a tool to test parameterization	17
2. 2. SCCM: the single-column version of CCM3	18
2.2.1 Governing equations of the SCCM.....	18
2.2.2 Parameterizations of the SCCM	19
2.2.3 Specifications of observed forcing	21
2. 3. Forcing data set: Model Initialization and boundary conditions	23
CHAPTER 3 - RESULTS AND DISCUSSION	26
3. 1. Simulations of standard cloud regimes	26
3.1.1 Low-level cloud fractions.....	28
3.1.2 Surface radiative fluxes	30
3.1.3 Profiles of temperature and moisture.....	34

	5
3.1.4 Surface fields.....	38
3. 2. Sensitivity to physical parameters and advective forcing.....	40
3.2.1 Influence of cloud type.....	40
3.2.2 Influence of the ice effective radius	43
3.2.3 Influence of the ice liquid ratio.....	47
3.2.4 Impact of forcing uncertainty	48
CHAPTER 4 - CONCLUSION.....	50
APPENDIX A: CLOUD PARAMETERIZATION	52
APPENDIX B: SYMBOL DEFINITION	55
REFERENCES	58

List of figures

Figure 1: Clouds effect on the radiative fluxes.	11
Figure 2: Observed annual cycle of the Arctic cloudiness.....	15
Figure 3: CCM3 simulation of the annual cycle of Arctic clouds.....	16
Figure 4: Schematic diagram of the SCCM.....	19
Figure 5: Cloud parameterization.....	20
Figure 6: Schematic of model forcing.....	23
Figure 7: Winter averages of simulated and observed low-level cloudiness.	28
Figure 8: Temporal evolution of the low-level cloud amount in standard simulations.	29
Figure 9: Frequency distribution of the observed and simulated cloud fraction.....	30
Figure 10: Temporal evolution of the downwelling LW radiative flux in standard simulations...	31
Figure 11: Mean and RMS error of downward LW fluxes.....	32
Figure 12: Temporal evolution of the upward LW radiative flux in standard simulation.	33
Figure 13: Winter average of the temperature profile.	35
Figure 14: Winter average of the moisture profile.	35
Figure 15: Temporal evolution of the error in temperature.....	37
Figure 16: Temporal evolution of the error in moisture.....	37
Figure 17: Time series of modeled surface temperature, sensible heat and latent heat fluxes.....	39
Figure 18: Impact of C3 clouds on the cloud fraction.	41
Figure 19: Impact of C3 clouds on the RMS error of the cloud fraction.....	42
Figure 20: Impact of the inversion strengths on the cloud fraction.	43
Figure 21: Impact of ice effective radius on downwelling LW flux.....	46
Figure 22: Impact of ice effective radius on cloud fraction.	46

Figure 23: Fraction of liquid phase in clouds..... 47

Figure 24: Sensitivity to advective forcing 49

List of tables

Table 1: Methods of specifying the large-scale forcing.....	22
Table 2: Variables included in the forcing data set.	25
Table 3: Observed and modeled parameters in standard simulations.....	27
Table 4: Means of downward LW fluxes.....	32

Acknowledgments

I would like to thank the people who have supported and helped me with this work. First, I thank my advisor Dr. Uma Bhatt for her continual support and encouragement in my research. She made this work really enjoyable through both her scientific and human qualities. I also acknowledge Dr. Jerry Harrington who instilled me with his interest of clouds and who supported me in this project through exciting discussions. I am grateful to Dr. Alexander Makshtas and Dr. David Newman for their meaningful comments on my work.

I thank the National Center for Atmospheric Research (NCAR) for providing the Single Column Model. I thank Christian Jakob and his coworkers at ECMWF for producing the ECMWF column dataset for SHEBA; Janet Intrieri, Matthew Shupe, Taneil Uttal, and their coworkers at NOAA/ETL for providing the radar and lidar datasets; Ed Andreas, Chris Fairall, Peter Guest, Ola Persson and their co-workers for providing the tower data set.

I also would like to thank all the other people who support me in many ways. In particular, I thank Vincent who listened to my daily chat about clouds during breakfast, and Dörte, during ski time. I am grateful to Igor for the liters of coffee and to Inna for the kilos of chocolate, without which this thesis could not have been completed. I highly appreciate the computing assistance I received from Chris Swingley.

This project was financially supported by the Frontier Research System for Global change and by the Center of Global Change & Arctic System Research at the University of Alaska Fairbanks, which are gratefully thanked.

CHAPTER 1 - INTRODUCTION

1.1. Cloud impacts on the radiative budget

Clouds play a fundamental role in the global climate system through their impacts on the radiative budget (Liou, 1992). They modify the earth's radiation budget by altering the absorption, scattering and reflection characteristics of the atmosphere. Cloud forcing provides a simplistic means for characterizing the bulk effect of clouds on the Earth's system. The longwave cloud radiative forcing, C_{LW} and the shortwave cloud radiative forcing, C_{SW} are defined (Ramanathan *et al.*, 1989) as follows:

$$\begin{aligned} C_{LW} &= F_{LW}(A_c) - F_{LW}(A_c = 0) \\ C_{SW} &= F_{SW}(A_c) - F_{SW}(A_c = 0) \end{aligned} \tag{1}$$

where F_{LW} and F_{SW} represent the net longwave and shortwave fluxes, respectively, and A_c is the cloud fraction. The values of the cloud forcing are negative for a cooling effect with respect to a clear sky and positive for a warming.

In general, clouds induce a negative shortwave forcing and a positive longwave forcing (Figure 1). In the visible, clouds reflect back to the space or absorb a significant amount of the incoming solar radiation. They reduce the solar absorption at the surface and the cloud impact in the shortwave energy budget is to cool the surface with respect to clear skies. C_{SW} is, hence, negative. In the longwave energy budget, clouds strongly absorb infrared radiation and they reduce the longwave radiation that returns back to space by filling in the atmospheric window. This yields a warming effect with respect to clear skies and to positive values of C_{LW} .

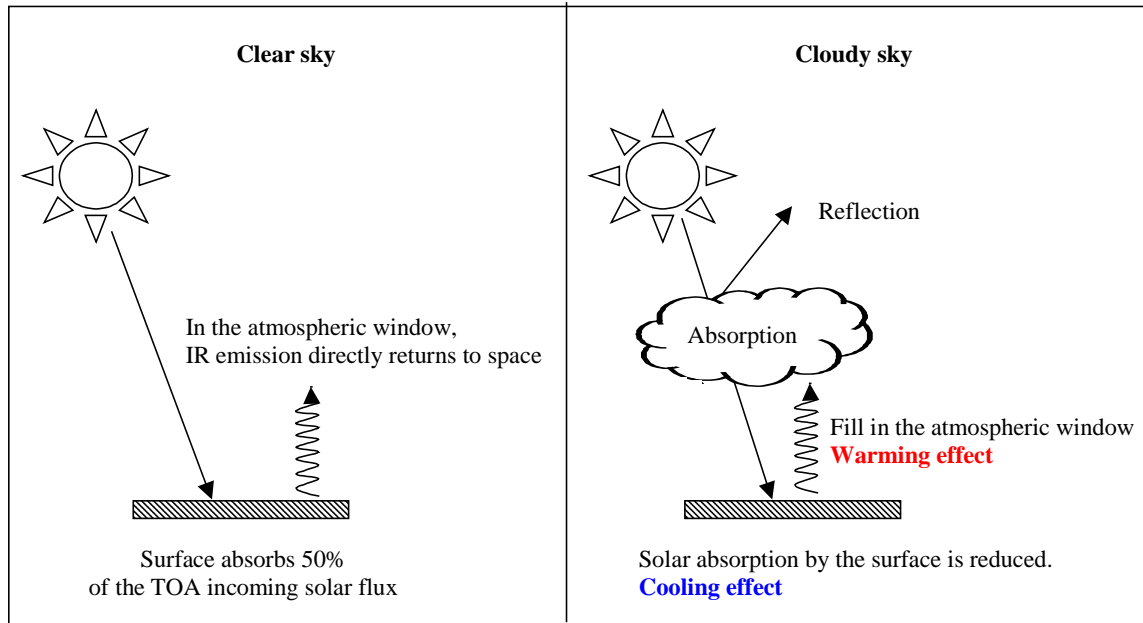


Figure 1: Clouds effect on the radiative fluxes. Clouds have a cooling effect in the shortwave budget and produce a warming in the longwave.

The net cloud radiative forcing C_{net} is the sum:

$$C_{net} = C_{LW} + C_{SW} \quad (2)$$

The net cloud radiative forcing C_{net} may be positive or negative depending on the type of clouds, the latitude and the time of the day. Globally, the net radiative effect of clouds is largely negative and clouds acts to cool the earth. In the Arctic, the role of clouds on climate differs from that in lower latitudes. There are specific characteristics of Arctic climate that are of importance for cloud impacts: the high albedo of snow and sea-ice, the frequent temperature inversions, the large amount of ice-phase in the low-level clouds, and the absence of solar radiation during wintertime.

The high reflectivity of snow and ice compared to vegetation and ocean has a direct effect on the shortwave radiative forcing. The cooling effect of clouds in the shortwave is somewhat reduced when compared to lower latitudes. Ramanathan *et al.* (1989) even found positive values of C_{SW} at the top of the atmosphere (TOA) over the Arctic suggesting that clouds might decrease

the albedo over bright snow-covered surfaces. This question has created some controverts as Nemesure *et al.* (1994) found the opposite, namely that clouds increase the albedo over snow-covered surfaces (see also Curry *et al.*, 1996).

In the Arctic, temperature inversions are frequent, especially during winter. In presence of a temperature inversion, the cloud top may be warmer than the surface. As a result, the loss of energy by infrared emission at the TOA may be larger under a cloudy sky than under clear sky. The longwave forcing, C_{LW} at the TOA may be negative and leads to a cooling with respect to clear skies, in contrast with lower latitudes.

Arctic clouds contain a large amount of ice phase especially during winter. The interactions between cloud and radiative fluxes are dependent on the cloud phase both in the longwave and in the shortwave. Cloud droplets form on Cloud Condensation Nuclei (CCN). The CCN for ice droplets differ from the liquid one, both in composition and number. Typically, the quantity of CCN for ice droplets is about 10^3 times less than for liquid droplets. The number of CCN influences the size and atmospheric lifetime of cloud droplets. As a result, for a given water density, we will have either many small liquid droplets or a few big ice droplets. At low temperature, any moisture entering the lower atmosphere probably would convert directly to big ice particles that fall out of the atmosphere rather than forming low clouds. Beesley *et al.* (1999) suggested that ice-fallout mechanism could explain the observations documenting the small amounts of low-level clouds in winter.

In the Arctic, it has been determined that clouds have a net warming effect on the surface except in the summertime (Curry *et al.*, 1992; Walsh *et al.*, 1998). The longwave effect of clouds prevails because of the absence of solar radiation during wintertime and due to the high surface albedo of sea-ice. The net effect of clouds in the Arctic contrasts with cloud forcing at lower latitudes, where there is a cooling at the surface with respect to clear sky.

1. 2. Arctic cloudiness characteristics

Clouds strongly influence the Arctic atmosphere and the surface budget through their interactions with IR and solar radiation. They should be properly represented in the Global Circulation Models (GCMs) in order to produce accurate predictions of climate. Tao *et al.* (1996) have found that most GCMs are unable to reproduce even the most basic features of the annual cycle of cloudiness over the Arctic Ocean, which is a concern for accurate predictions of Arctic climate.

The present section gives a brief review of the climatology of cloud fraction over the Arctic Ocean. The observations are then compared with the simulated cloud fraction from the Climate System Model (CSM) from the National Center for Atmospheric Research (NCAR).

1.2.1 Observed climatologies of Arctic cloudiness

Relevant observations of the cloudiness over the Arctic Ocean are very restricted and the observational estimates contain large uncertainties. Characteristics of the Arctic cloudiness have been described by among others in Curry *et al.* (1996), Walsh *et al.* (1998) and Intrieri *et al.* (2001b). Figure 2 shows the annual cycle of the Arctic cloudiness observed with different techniques: surface observations, satellite data and combined lidar-radar measurements. The cloud fraction obtained from the surface observations and satellite data refers to the fractional area of the sky that is covered by clouds while in the radar/lidar data refers to the time-averaged that a cloud is overhead.

The surface observations of cloud amount shown in Figure 2 were obtained from Clark *et al.* (1996). The cloud fraction corresponds to the monthly average value over the Arctic Ocean. It has been derived from surface observations performed by Russian drifting ice stations during the 1950-91 period. The observed cloudiness displays a large seasonal cycle between winter and summer. The maximum cloudiness occurs during the summer months with mean cloud fractions of about 0.8, while the lowest cloudiness is during winter with mean wintertime values around

0.5. It has been pointed that surface observations may underestimate the cloud cover, especially during winter. Two factors may act to underestimate winter cloud cover: first, clear-sky ice crystal precipitation is usually not reported in present cloud classifications (Curry *et al.*, 1996) and secondly, visual observations of clouds are hindered during polar night due to inadequate illumination of clouds (Hahn *et al.*, 1995).

Figure 2 also shows cloud fraction determined from the combined radar and lidar data set measured during the SHEBA experiment (Intrieri *et al.*, 2001b). The cloud fraction measured at the SHEBA site shows a pronounced annual cycle, as do surface-based observations shown above. However, the values of cloud fraction are larger at SHEBA. Intrieri *et al.* (2001b) pointed out that SHEBA year was cloudier than average because it was particularly stormy due to the 1997-98 El Nino event. The transition in cloud fraction in spring and in fall occurs earlier at SHEBA site than for the surface-based observations.

The satellite cloud climatology shown in Figure 2, was provided by Key *et al.* (1999). No annual cycle is apparent and the cloud fraction is around 0.7 all the year. This climatology has been generated with an improved cloud detection algorithm for the Polar Regions. But the determination of polar cloudiness by satellite observations still encounters significant difficulties. The satellites are operating near the limit of their performance range for surface temperatures (Minnis *et al.*, 2001). The difference between the cloud-top and surface and between the cloud and surface albedos is small. Moreover, satellite estimates of the cloud cover may be overestimated because they include low-level ice crystal precipitation (Curry *et al.*, 1996).

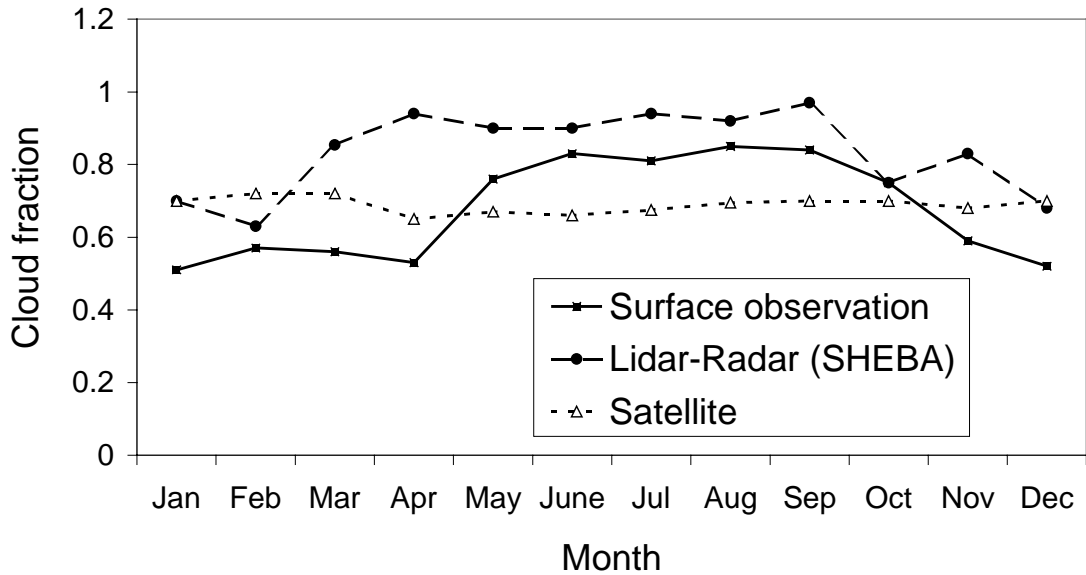


Figure 2: Observed annual cycle of the Arctic cloudiness.

The cloud fraction was observed with different techniques: surface observations, satellite data and combined lidar-radar measurements. The cloud fraction obtained with surface observations and satellite data refers to the fractional area of the sky covered by clouds while in the radar/lidar data set, it refers to the time-averaged probability to have a cloud is overhead.

1.2.2 Prediction of Arctic cloud cover by GCMs

Tao *et al.* (1996) have compared the Arctic cloudiness simulated by 19 GCMs in the Atmospheric Model Intercomparison Project (AMIP). They showed that the simulated cloudiness varies enormously from model to model. Some models capture the seasonal cycle, at least qualitatively but others show an increase of the cloud cover in winter, which is qualitatively opposite to the observations.

We have evaluated the Arctic cloudiness predicted by the CSM2 from NCAR. CSM is a comprehensive coupled model of the Earth's climate system with sea-ice, ocean, atmosphere, and land models. The atmosphere component of the CSM is the Climate Community Model (CCM

3.6). Simulated cloud fraction data were taken from the 300-year simulation from the fully coupled simulation of CSM (b003). Figure 3 shows the simulated cloud fraction over the Arctic Ocean for latitude higher than 70 N. For an easy comparison, it also includes the surface-based observed cloudiness. Clearly, the model does not capture the seasonal cycle. The simulated cloud cover is maximum during winter and largely overestimated the observations with values up to 0.95. During summertime between May and September, simulated cloudiness matches observations more accurately with an error between -7% to 4% .

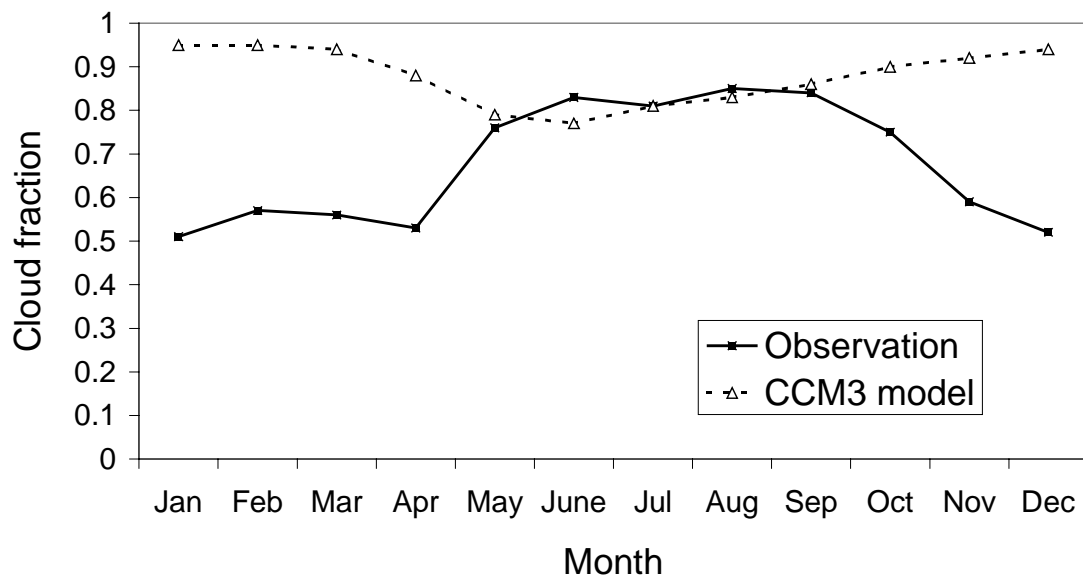


Figure 3: CCM3 simulation of the annual cycle of Arctic clouds.

The simulated cloud fraction corresponds to the dashed line, while the surface-based cloudiness observed by Clark et al. (1996) is shown in plain.

As a whole, CCM3 is unable to reproduce the annual cycle of Arctic cloud amount. In particular, the model is very inaccurate during the wintertime with large overestimates of observations. The primary objectives of this work are to answer the following:

- Why does CCM3 overestimate the Arctic cloudiness during winter?
- Which modifications of the cloud parameterization may improve the simulations?

CHAPTER 2 - MODEL DESCRIPTION

As discussed in the introduction, the CSM from NCAR produces an unrealistic simulation of Arctic clouds during winter and the main purpose of this study is to test the cloud parameterization of CCM3, the atmosphere component of CSM. The cloud parameterization is evaluated using the Single-column version of CCM3, the SCCM. Single-column Model (SCM) forced with observations is a tool commonly used to evaluate parameterizations of global models. In this chapter, we present the modeling framework, its strengths and weaknesses, the governing equations and parameterizations in the model, the methods and the data sets used to force the model.

2.1. Single-Column model: a tool to test parameterization

The quality of the simulations of Global Climate Models (GCMs) depends on the physical parameterizations in the model (i.e. the representations of the physical processes that occur on the scales smaller than the model grid). Much effort has been gone into improving GCMs parameterizations.

Testing parameterizations through simulations of the GCM itself is computationally expensive and time-consuming. An alternate economic approach is to test parameterizations of large-scale models using a SCM. Betts *et al.* (1986) pioneered the use of SCMs as a tool for testing parameterizations of large-scale models. Since then, this method has been widely used (Beesley *et al.*, 1999; Hack *et al.*, 2000; Pinto *et al.*, 1999). Randall *et al.* (1996, 1999) present a complete discussion of the strategies for testing parameterizations with SCMs.

A SCM is essentially a single grid column of a global model extracted from its environment (Figure 4). Observations are used to specify the conditions in the neighboring columns. The SCM contains time-dependent equations and parameterizations similar to those of a vertical column of the GCM. The horizontal feedbacks that occur in global models are taken into account by

prescribing time-dependent boundary conditions derived from observations. Therefore, the state of the column of the SCM depends on both the prescribed boundary conditions and on the physical processes occurring within the column.

A SCM is an easy and inexpensive method to evaluate parameterizations without the complications from feedbacks from other components of the model. However, there are some problems with SCMs. First, it has demanding data requirements and the time-averaged total tendencies need to be accurate in order to prevent an accumulation of errors. Additionally, SCMs lack the complete feedback mechanics occurring in GCMs, as a result, problems that involve such a feedbacks cannot be detected. So, it is difficult to predict the behavior of a parameterization based solely on SCM tests. However, this method provides an inexpensive first look at the characteristics of a given parameterization.

2. 2. SCCM: the single-column version of CCM3

The cloud parameterization of CCM3 is evaluated with the SCCM, which is the single-column version of CCM3. A schematic of the SCCM is shown in Figure 4 and a complete description may be found in Hack *et al.*, (1999). We describe here briefly the set of equations governing the model, its parameterizations and the method used to force the model in this study.

2.2.1 Governing equations of the SCCM

The SCCM is governed by prognostic equations for temperature, moisture and horizontal winds. As the SCCM lacks the horizontal feedbacks, the governing equations are coupled only through the parameterized physics. It means that the thermodynamics and momentum components of the governing equations are independent of each other and we may only treat the thermodynamic budget.

$$\frac{\partial T}{\partial t} = -\mathbf{V} \cdot \nabla T - \omega \frac{\partial T}{\partial p} + \omega \frac{RT}{p c_p} + Q_{phys} \quad (3)$$

$$\frac{\partial q}{\partial t} = -\mathbf{V} \cdot \nabla q - \omega \frac{\partial q}{\partial p} + S_{phys} \quad (4)$$

The terms subscripted by “phys” denote the collection of parameterized physics terms, which is identical to the standard package of CCM3.6 (Kiehl *et al.*, 1996).

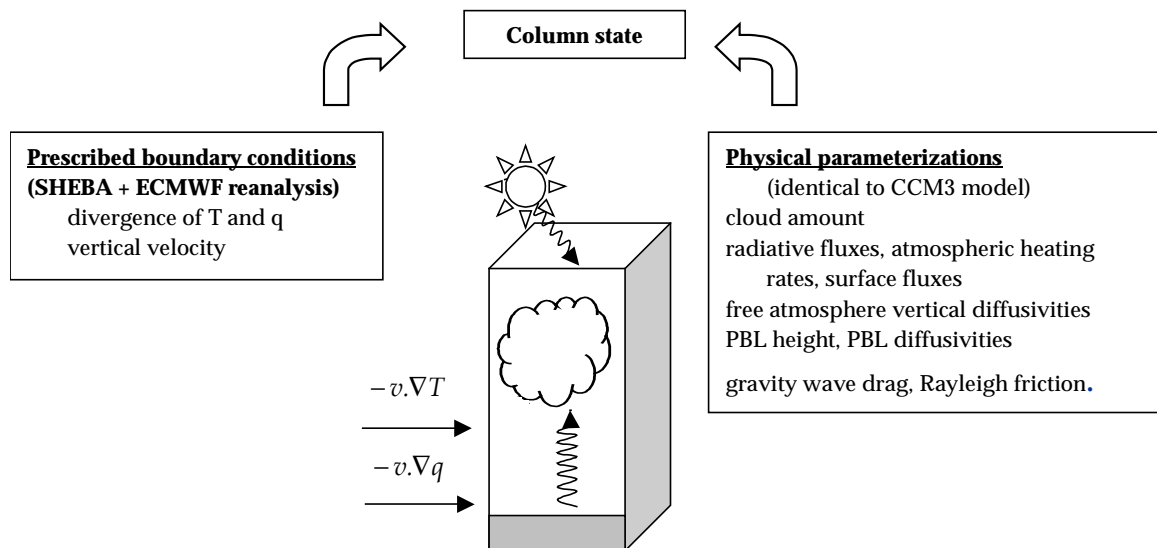


Figure 4: Schematic diagram of the SCCM.

The state of the column depends on both the prescribed boundary conditions taken from the observations and on the physical processes occurring within the column.

2.2.2 Parameterizations of the SCCM

The CCM3.6 parameterization packages include the parameterization of cloud amount, the evaluation of radiative fluxes and atmospheric heating rates; the evaluation of surface fluxes; update land surface properties; evaluation of free atmosphere vertical diffusivities, diagnosis of the PBL height, PBL diffusivities and non-local transport term followed by the vertical diffusion solution; evaluation of gravity wave drag tendencies and Rayleigh friction (Kiehl *et al.*, 1996)

We are interested in the cloud parameterization of CCM3, which is shown schematically in Figure 5. A full description of the cloud parameterization may be found in Appendix A. The cloud amount and the associated optical properties are evaluated via a diagnostic method that follows schemes developed by Slingo (1987, 1989). Three types of clouds are diagnosed by the scheme: convective (C1), layered (C2) and stratus associated low-level inversions of temperature and moisture (C3). The diagnosis of cloud fraction depends on relative humidity, vertical velocity, atmospheric stability and the convective mass flux associated with parameterization of moist convection.

The cloud optical properties are calculated using the cloud liquid water path and the cloud effective radius. Over the ocean, the liquid effective radius is set to $10\ \mu\text{m}$ and the ice effective radius varies between $10\ \mu\text{m}$ and $30\ \mu\text{m}$ and is a function of elevation. The clouds are in liquid phase above -10C , in ice phase below -30C , and in mixed phase between these temperatures, with the fraction of ice depending linearly on the temperature.

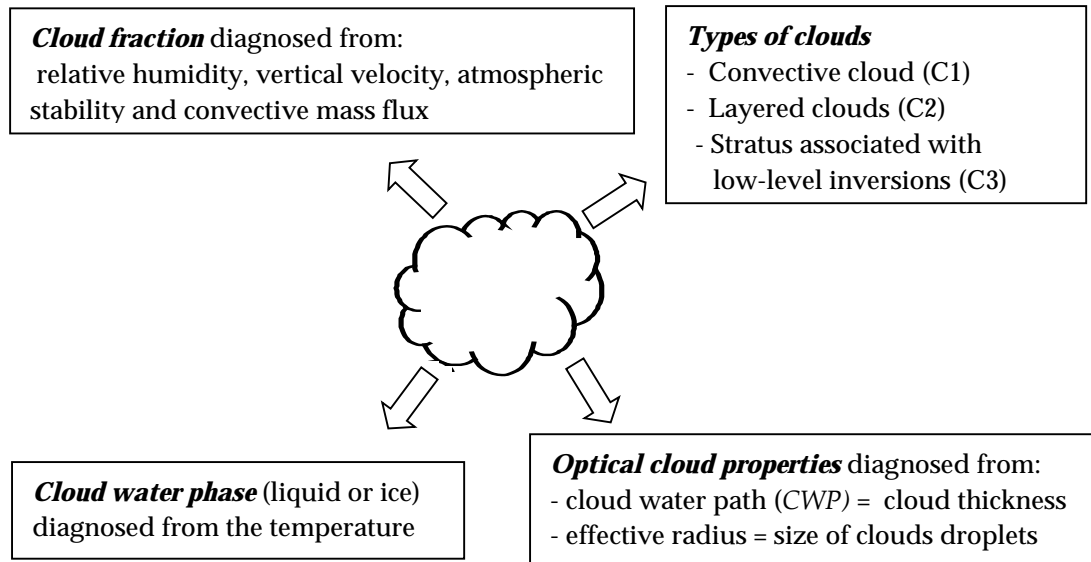


Figure 5: Cloud parameterization.

The cloud amount and the optical properties are diagnosed from Slingo parameterization

2.2.3 Specifications of observed forcing

The SCCM numerically integrates the prognostic equations of T and q , starting from an initial condition derived from observations and prescribing the large-scale forcing also from the observations. The different terms of the right-hand side of the equations (3) and (4) are either evaluated numerically or are specified. We used four methods of forcing the SCM: revealed advection (*3D*), horizontal advection (*2D*), prescribed surface fields (*sfc*), relaxation to the observed temperature and moisture (*relax*). These forcing methods of specifying the large-scale forcing are described in Figure 6 and in Table 1.

We can write the equations of the thermodynamics budget in the generic form:

$$\frac{\partial x}{\partial t} = -\mathbf{V}\cdot\nabla x - \omega \frac{\partial x}{\partial p} + X_{phys} \quad (5)$$

where x represents T , q .

The **revealed forcing (3D)** consists of computing the 3D advection $-(\mathbf{V}\cdot\nabla x + \omega \partial x/\partial p)$ directly from the observations and then prescribing these values in the SCM.

$$\frac{\partial x}{\partial t} = -(\mathbf{V}\cdot\nabla x + \omega \frac{\partial x}{\partial p})_{obs} + X_{phys} \quad (6)$$

This revealed forcing approach is very simple but it fails to take into account how simulated changes in the sounding would affect the tendencies due to vertical advection

The **horizontal advective forcing (2D)** consists of prescribing the horizontal advection $-(\mathbf{V}\cdot\nabla x)$ and ω from the observations, ω being computed from the profile of divergence using the continuity equation. The predicted value of x is then used to evaluate $-(\partial x/\partial p)$. So we have:

$$\frac{\partial x}{\partial t} = -(\mathbf{V}\cdot\nabla x)_{obs} + \omega_{obs} \frac{\partial x}{\partial p} + X_{phys} \quad (7)$$

The surface fields (surface temperature, sensible and latent heat fluxes) may be either predicted by the model or prescribed from the observations. In the *2D* and *3D* experiments, the surface fields are computed by the SCCM using the surface fluxes parameterizations. In the **prescribed surface field forcing (sfc)**, the surface fields are prescribed from the observations, in

addition to the horizontal advective forcing, in order to see more specifically how the model is dealing with clouds and radiative fluxes.

In the **relaxation forcing (relax)**, a relaxation term is added to the right side of the equation (5). The forcing terms also includes the horizontal advection of T and q and the prescribed surface fields. We may write:

$$\frac{\partial x}{\partial t} = -(\mathbf{V} \cdot \nabla x)_{obs} + \omega_{obs} \frac{\partial x}{\partial p} + X_{phys} + \frac{x_{obs} - x}{\tau} \quad (8)$$

where x_{obs} is the observed value of x and τ a specified “relaxation timescale” which was typically set to 3 hours. The effect of the relaxation term is to prevent the predicted value of x from drifting too far away from the observed value. A problem is that relaxation term does not represent any real physical process. But this approach is interesting as it allows us to examine how well the model is representing the clouds and the surface radiative fluxes when realistic soundings are used.

Table 1: Methods of specifying the large-scale forcing.

There are four methods of forcing the SCM: revealed advection (3D), horizontal advection (2D), prescribed surface fields (sfc), relaxation to the observed temperature and moisture (relax).

Label	Forcing terms
3D	Revealed forcing
2D	Horizontal advective forcing
Sfc	Horizontal advective forcing + Prescribed surface condition
relax	Horizontal advective forcing + Prescribed surface condition + Relaxation of T and q to the observations

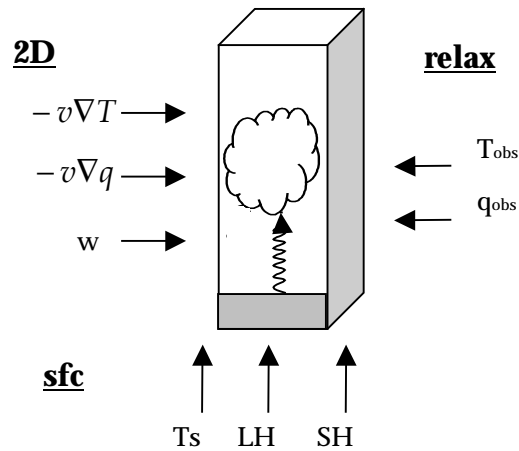


Figure 6: Schematic of model forcing.

In the 2D forcing, are prescribed horizontal advections of T and q , as well as vertical velocity. In sfc forcing, we also prescribe the surface fields (sfc). In the relax forcing, we relax T and q to the observations additionally.

2. 3. Forcing data set: Model Initialization and boundary conditions

The SCM is initialized and forced with a forcing data set, which is a compilation of both observations and reanalysis data. Observations were obtained from the Surface Heat Budget of the Arctic Ocean (SHEBA) experiment. The SHEBA program collected data from October 1997 to September 1998 (Perovich *et al.*, 1999). The reanalysis was integrated with the forecast model of the ECMWF (European Centre for Medium-Range Weather Forecasts) which has a package of physical parameterization that are at least as sophisticated as most GCMs (ECMWF Research Department, 1988; 1991; Beesley *et al.*, 2000). The ECMWF reanalysis was performed by assimilating the observations into the forecast model to reinitialize each daily forecast cycle.

Observations and reanalysis data have both their own advantages and disadvantages. The advantage of the reanalysis is that it incorporates all available data from diverse fields to produce

a dynamically consistent dataset. The reanalysis also gives values for variables that are difficult to measure directly such as the large-scale vertical motion and the advective tendencies of heat and moisture. On the other hand, the reanalysis may give unreliable values for some variables if the corresponding parameterizations leading to these variables are inaccurate. An evaluation of the ECMWF reanalysis against the observations may be found in Bretherton *et al.* (2001) and Beesley *et al.* (2000).

The forcing data set contains all the variables shown in Table 2. The origin and reliability of each variable is discussed below.

The longitude and latitude of SHEBA location varied but for simplicity, we used monthly averages of location in the forcing datasets. We may afford this simplification because the radiative fluxes of the simulated period are only longwave fluxes. If solar radiation were present, this procedure would be inaccurate as even small differences in solar parameter such as solar zenith angle at high latitude may contribute to large discrepancies in the cloud forcing (Intrieri *et al.*, 2001a).

Inside the column itself, the ECMWF reanalysis provides values for prescribing air temperature, moisture, advective tendencies, surface pressure, vertical velocity, wind speed, when needed. Following Bretherton *et al.* (2001) we assume that the ECMWF values of these variables are good enough to force the SCM. Bretherton *et al.* showed the model wind and temperature fields are quite close to the sounding measurements. The other fields show some small sharp jumps at periodic intervals due to the effects of corrected initial conditions on the forecasts, but the errors remain within acceptable limits.

The surface fields i.e. surface air and ground temperatures, sensible and latent heat fluxes, are taken directly from the observations because near the surface, the ECMWF model produces large errors in the surface fields (Bretherton *et al.*, 2001). For example, the predicted surface air temperature is damped during winter with respect to observations, which is attributed to the sea-ice model that treats sea-ice as an isothermal slab with a large thermal inertia preventing rapid changes in the surface air temperature.

Table 2: Variables included in the forcing data set.

The “category” tell if a given variable is computed by the SCCM, or if it is prescribed or relaxed to the observations. The “provenance” tells if the variable is taken from gross observations of SHEBA, or from the ECMWF reanalysis. The “averaging” tells is the value corresponds to the hourly or to a monthly average.

Complete Name	Units	Category	Provenance	Averaging
Time	S	prescribed	-	1 hour
Pressure Levels	Pa	prescribed	31 levels	constant levels
Latitude	deg N	prescribed	Observations	Monthly
Longitude	deg E	prescribed	Observations	Monthly
Temperature	K	computed or relaxed to observations	ECMWF	Hourly
Horizontal T advective tendency	K/s	prescribed	ECMWF	Hourly
Vertical T advective tendency	K/s	prescribed or computed	ECMWF	Hourly
Specific humidity	kg/kg	computed or relaxed to observations	ECMWF	Hourly
Horizontal Q advective tendency	kg/kg/s	prescribed	ECMWF	Hourly
Vertical Q advective tendency	kg/kg/s	prescribed or computed	ECMWF	Hourly
Surface Pressure	Pa	prescribed	ECMWF	Hourly
Vertical Pressure Velocity	Pa/s	prescribed	ECMWF	Hourly
Surface Pressure Tendency	Pa/s	prescribed	ECMWF	Hourly
U Windspeed	m/s	prescribed	ECMWF	Hourly
V Windspeed	m/s	prescribed	ECMWF	Hourly
Ground Temperature	K	prescribed or computed	Observations	Hourly
Surface air temperature	K	prescribed or computed	Observations	Hourly
Surface sensible heat flux	W/m ²	prescribed or computed	Observations	Hourly
Surface latent heat flux	W/m ²	prescribed or computed	Observations	Hourly

CHAPTER 3 - RESULTS AND DISCUSSION

In this chapter, we present results from single-column model simulations forced with data from the SHEBA experiment. The period from November to January has been chosen for the simulations because simulated clouds from the global NCAR CSM are farthest from observed climatology during winter, as discussed in section 1. 2.1.2.2.

We have performed 2 types of SCM experiments: standard simulations and sensitivity studies of the cloud parameterization. The standard simulations in the winter months have been conducted using the standard parameterization packages of CCM3, i.e. without any modification of the existing cloud parameterization. In the sensitivity studies, we look at the impact of varying cloud type, ice effective radius and ice liquid ratio in clouds as well as the advective forcing uncertainty.

We evaluate the simulated cloud fraction, longwave radiative fluxes, temperature and moisture profiles, and surface fields against with the observations. In our discussion, the different forcing methods are follow the descriptions given in section 2. 2.2.2.3: revealed forcing (*3D*), horizontal forcing (*2D*), prescribed surface properties (*sfc*), relaxation forcing (*relax*). Moreover, we use the denomination (*non-relax*) to refer to *3D*, *2D* and *sfc* forcing.

3. 1. Simulations of standard cloud regimes

Mean values and RMS error for cloud fraction, longwave radiative fluxes, temperature and moisture profiles, and surface fields during November-January are shown in Table 3.

The mean and the RMS error of a field f is defined as:

$$Mean = \sum_{i=1}^N \frac{f_{model}^i}{N} \quad (9)$$

$$RMSE = \sqrt{\sum_{i=1}^N \frac{(f_{model}^i - f_{observation}^i)^2}{N}} \quad (10)$$

where f_{model}^i and $f_{observation}^i$ are the simulated and observed values of f at the i^{th} time step of the simulations and N is the total number of time steps. The RMSE provides a measure of the total difference between the simulations, thus helps to evaluate the simulation quality.

Quality of the simulations of cloud fraction, longwave radiative fluxes, temperature and moisture profiles, and surface fields are discussed in the following sections. The 3D forcing simulations do not yield qualitatively different results from the 2D forcing. We only show the 2D results, except when there are qualitative differences between the 2D and 3D simulations.

Table 3: Observed and modeled parameters in standard simulations.

Mean and RMSE are given for the period November-January for: low-level cloud fraction (Ac), downwelling longwave flux at the surface (LWd), upwelling longwave flux at the surface (LWu), surface temperature (Ts), sensible heat flux (SH), latent heat flux (LH).

		2D	3D	Sfc	Relax	obs
Ac	Mean	0.81	0.79	0.72	0.46	0.53
	RMSE	0.52	0.45	0.50	0.30	
LWd (W/m ²)	Mean	198	202	187	171	179
	RMSE	38	39	27	21	
LWu (W/m ²)	Mean	219	224	205	205	204
	RMSE	23	28	-	-	
Ts	Mean	249	251	244	244	244
	RMSE	8	9	-	-	
SH (W/m ²)	Mean	-2	-4	-5	-5	-5
	RMSE	17	16	-	-	
LH (W/m ²)	Mean	11	11	-0.1	-0.1	-0.1
	RMSE	13	14	-	-	

3.1.1 Low-level cloud fractions

Figure 7 shows the low-level cloud fraction averaged over the December and January period and Figure 8 gives the temporal evolution of the daily low-level cloud amount, over the winter months. The simulated low-level cloud amount is compared to the cloud fraction occurrence measured by a lidar system at SHEBA (Intrieri *et al.*, 2001b). As the lidar measurements may be severely attenuated by the absorption of large ice particles or by optically thick clouds, we consider that the lidar measurements of the cloud amount better represent the low-level cloud cover rather than the total cloudiness. It is why the lidar values are compared to the simulated low-level cloud fractions.

The horizontal advective forcing simulation (2D) overestimates the winter cloud cover, as does the revealed forcing (not shown). Moreover, the SCCM does not capture correctly the temporal evolution of cloudiness in these simulations. Prescribing the surface fields (*sfc*) slightly improves the simulations of the low-level clouds. However, the cloud fraction is still considerably overestimated. When the relaxation term is used, the SCCM reproduces fairly well the low-level cloud cover, both in terms of average value and temporal evolution. It appears that reproducing the temperature and moisture profiles is crucial for capturing the cloud cover evolution. If T and q are accurate, the cloud parameterization of CCM3 works fairly well to reproduce the cloudiness over SHEBA.

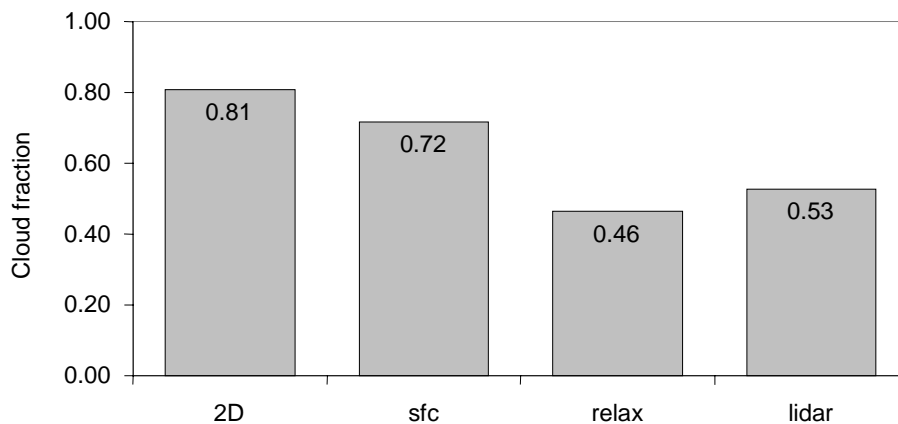


Figure 7: Winter averages of simulated and observed low-level cloudiness. The low-level cloud fraction is averaged over the December and January period.

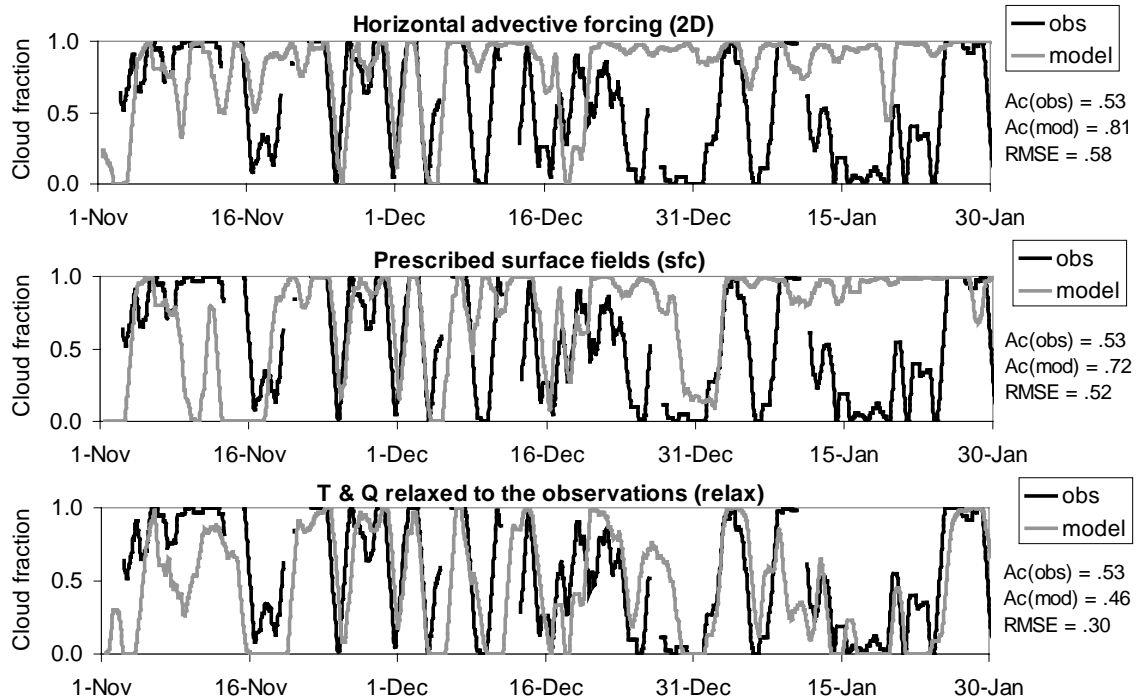


Figure 8: Temporal evolution of the low-level cloud amount in standard simulations. Daily averages are given; the black lines represent the observed values (lidar observations) and the gray lines the modeled values (2D, sfc and relax simulations). Mean values and RMSE are given on the right.

Another interesting characteristic of the Arctic clouds is that they have a highly bimodal distribution (Makshtas *et al.*, 1999; Walsh *et al.*, 1998). Clear sky or overcast sky situations are statistically more probable than a partial cloud cover. As shown in Figure 9, this characteristic is observed in the lidar measurements at SHEBA during the considered period. Once again, an accurate prediction of the temperature profiles is crucial for reproducing this characteristic in the simulations. The *non-relax* simulations yield a too large frequency of the totally covered sky. However, the *relax* experiment overestimates the frequency of partly cloudy skies (i.e. cloud amount between 0.2 and 0.8)

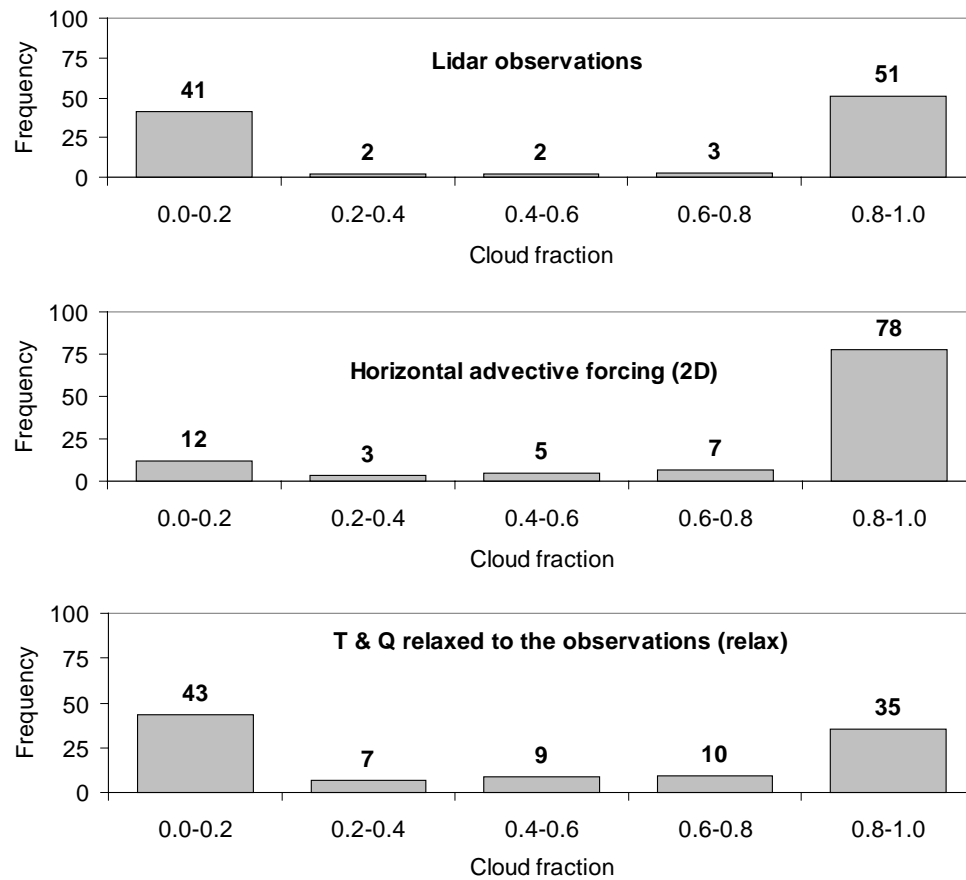


Figure 9: Frequency distribution of the observed and simulated cloud fraction. The histogram gives the frequency distribution by increment of 0.2 in cloud fraction. Frequency distributions are given for lidar observations, 2 D and relax simulations. The time resolution is one hour.

3.1.2 Surface radiative fluxes

The longwave radiative flux is a vital component of the surface energy budget during the Arctic winter. We discuss in section 1.1 how clouds affect the longwave radiative fluxes at the surface: clouds absorb and emit longwave radiation and as a result, they increase the downwelling LW radiation. This increase is especially significant in the Arctic where atmospheric conditions are typically dry and thus less opaque to LW radiation. The downward longwave radiative fluxes at the surface are given in Figure 10 for the 2D, *sfc* and *relax* forcing experiments. As previously, the simulations improve gradually when the surface fields are prescribed and

when T and q are relaxed to the observations, with an RMS error, decreasing from $\text{RMS} = 38$ W/m^2 to $\text{RMS} = 21$ W/m^2 . A comparison between the times series of the cloud fraction (Figure 8) and the downwelling LW flux (Figure 10) shows that an overestimate of the cloud fraction yields an overestimation of the downwelling flux. This is expected from the fact that clouds increase the downwelling LW radiative flux. For example, the 2D forcing produces too much clouds during the periods from 12/20/1997 to 1/4/1998 and 1/13/1998-1/25/1998. As a result the downwelling LW flux is overestimated during these periods.

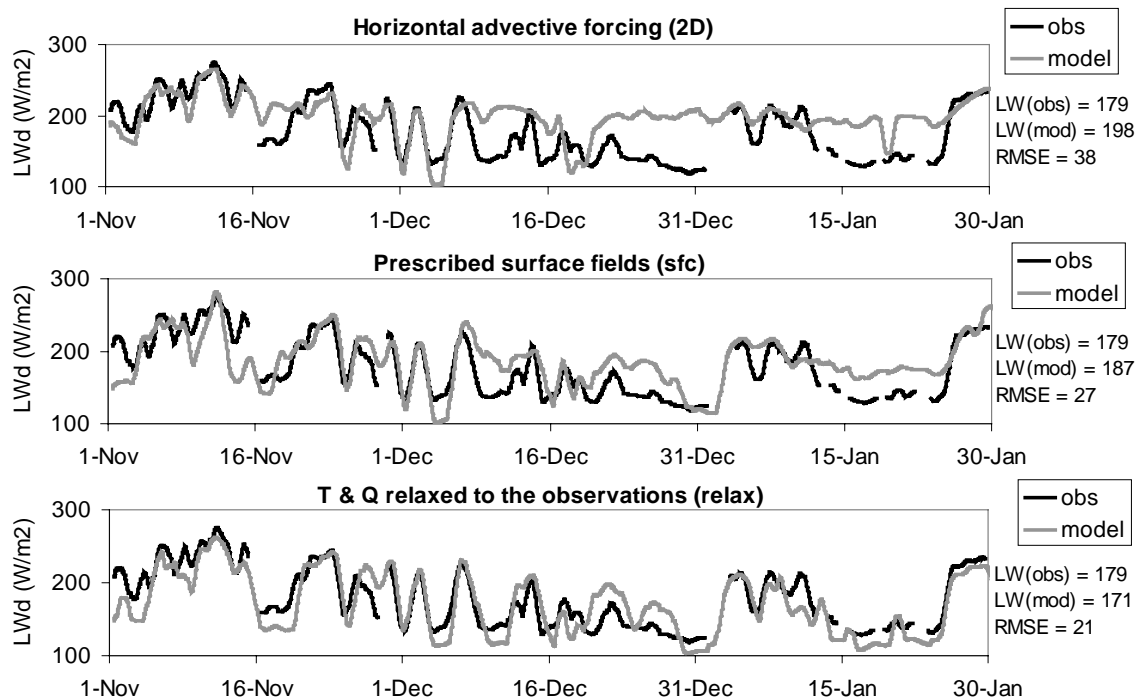


Figure 10: Temporal evolution of the downwelling LW radiative flux in standard simulations. Daily averages are given; the black lines represent the observed values (lidar observations) and the gray lines the modeled values (2D, sfc and relax simulations). Mean values and RMSE are given on the right.

Table 4 and Figure 11 compares the performances of the model under clear skies towards cloudy skies. Table 4 gives the simulated downward LW fluxes to the observations for clear and cloudy periods. The RMS error is given in Figure 11. The downward LW fluxes are split between

clear sky periods (cloud fraction lower than 0.2) and cloudy periods (cloud fraction larger than 0.8). The observed downward LW flux is 140 W/m² under clear skies and it increases by 60 W/m² under cloudy skies, due to the cloud absorption in LW radiation. The 2D forcing overestimates clear and cloudy downwelling LW fluxes. The RMSE for 2D forcing is the largest for clear sky periods. Prescribing the surface conditions (*sfc*) improves the simulations but the LW fluxes under clear skies are still overestimated. Adding the relaxation term to observed T and q profiles yields best simulations of the downward LW fluxes, and in this case, the simulations under clear skies are as accurate as the cloudy skies.

Table 4: Means of downward LW fluxes.

Means are for the period November through January. The overall fluxes are given, the flux under clear and cloudy skies as well as the difference between clear and cloudy skies.

	Observation	2D	Sfc	Relax
	F_{LW} (W/m²)	F_{LW} (W/m²)	F_{LW} (W/m²)	F_{LW} (W/m²)
Overall(Ac = 0 - 1)	177	199	187	172
Clear sky (Ac = 0 - 0.2)	143	189	170	142
Cloudy sky (Ac = 0.8 - 1)	203	207	204	194
Difference between clear-cloudy	60	18	34	52

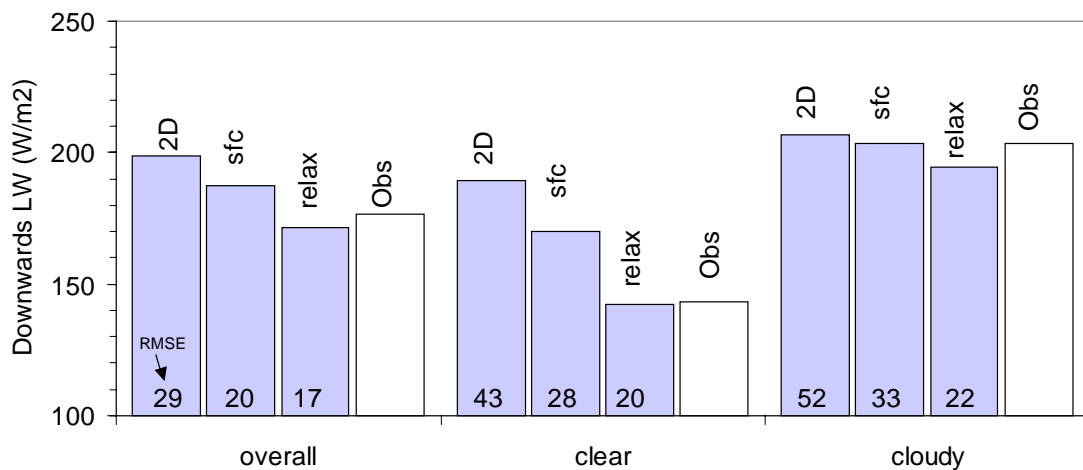


Figure 11: Mean and RMS error of downward LW fluxes.

Means are for the period November through January. The RMSE are given in the inside base.

The upward longwave flux is calculated using the Stefan Boltzman's law based on the surface temperature of the ice, T_s :

$$F_{LW}^u = \sigma T_s^4 \quad (11)$$

It means that the SCCM reproduces the upward flux fairly well when the surface temperature is prescribed from the observations, i.e. for *sfc* and *relax* experiments (not shown here). In the *2D* experiment, the surface temperature is computed by the SCCM by assuming a 2-meter sea-ice slab at the lower boundary. The upwelling LW flux is deduced from T_s from equation (11). As shown in Figure 12, the model overestimates of the upwelling LW flux especially during the clear sky periods. This is due to errors in the surface temperature, as discussed in section 3. 1.3.1.4.

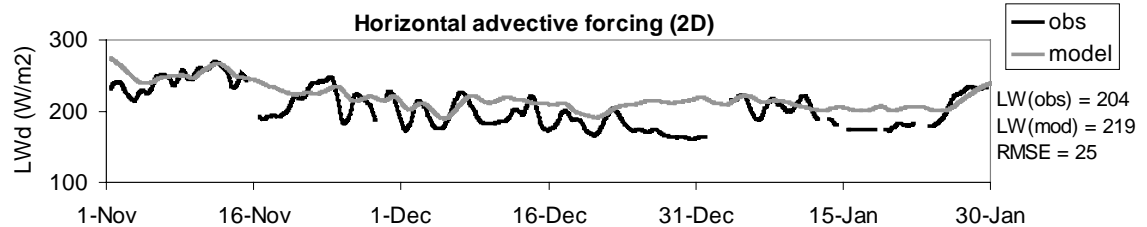


Figure 12: Temporal evolution of the upward LW radiative flux in standard simulation. Daily averages are given; the black lines represent the observed values and the gray lines the modeled values (2D, *sfc* and *relax* simulations). Mean values and RMSE are given on the right.

3.1.3 Profiles of temperature and moisture

As discussed in the previous section, accurate temperature and moisture profiles are critical for reproducing cloud fraction and LW fluxes accurately at the surface. In Figure 13 and Figure 14, we examine these profiles integrated with *2D*, *3D* and *sfc* forcing and we evaluate them through a comparison with the ECMWF reanalysis. *Relax* forcing is naturally omitted for T and q simulations. The profiles are averaged over the winter months (November to January). Above the surface, the ECWMF values are quite close to sounding measurements (Bretherton *et al.*, 2001), and we use ECWMF values to avoid the complications of missing values. The observed temperature and moisture profile show strong inversions under 850 mb. The model encounters difficulties reproducing these inversions, no matter which the forcing method is used. Above 800 mb, the winter temperature and moisture bias are fairly small, in average.

The revealed forcing (*3D*) produces less accurate temperature but better moisture profiles than the horizontal forcing (*2D*). As discussed in section 3. 1. 3.1.4., the SCCM simulates unrealistic surface fields. As a result, prescribing the surface properties (*sfc* forcing) improves the thermodynamic profiles in the boundary layer, particularly the moisture.

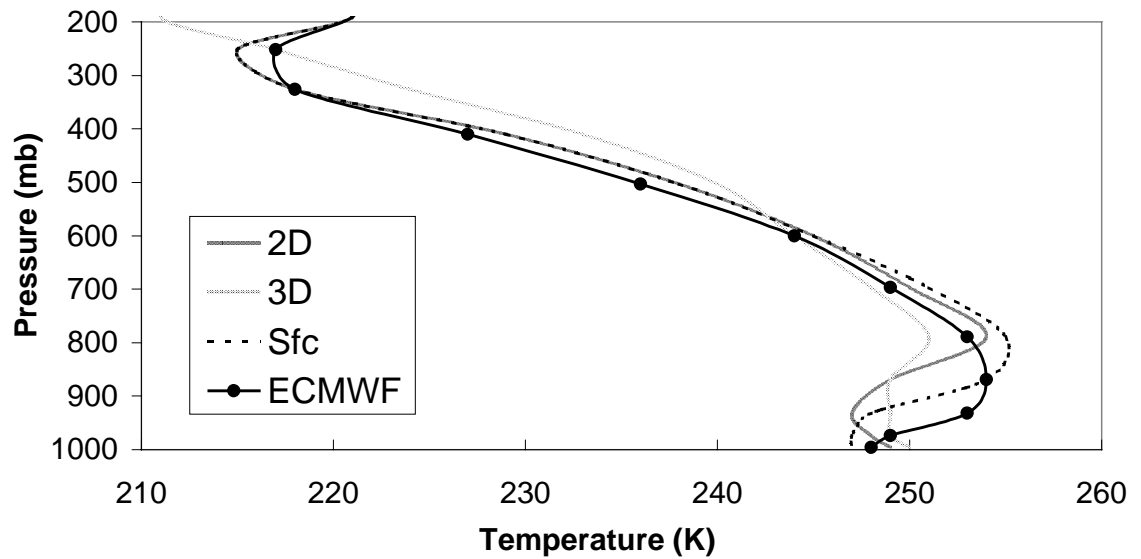


Figure 13: Winter average of the temperature profile.
 Simulations (2D, 3D and sfc) are evaluated against the ECMWF data.

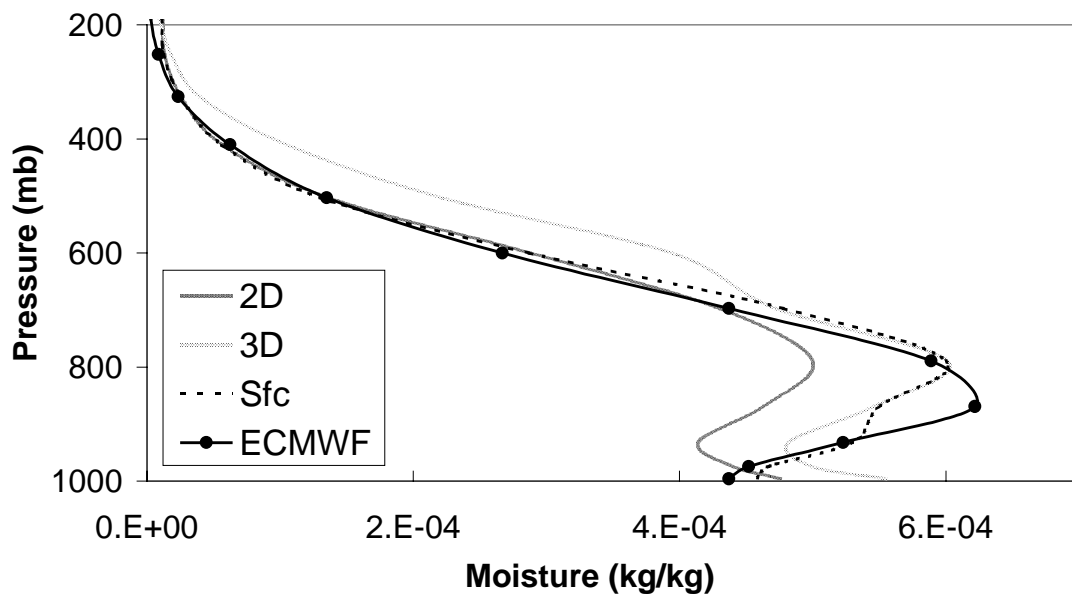


Figure 14: Winter average of the moisture profile.
 Simulations (2D, 3D and sfc) are evaluated against the ECMWF data.

In addition to the average profiles, we also evaluated the temporal evolution of the temperature and moisture errors by comparing with the observed values. The temperature error is defined as:

$$\Delta T = T_{model} - T_{observation} \quad (12)$$

and the moisture error defined as:

$$\Delta q = q_{model} - q_{observation} \quad (13)$$

The error in T and q profiles integrated with 2 D forcing is shown in Figure 15 and Figure 16, respectively. It appears that, below 800 mb, the model is constantly too cold with respect to observations, which is reproduced by the average profile. On the other hand, above 800 mb, alternating periods of anomalously cold and warm biases occur. The accuracy of the winter average is an artefact due to the compensation of errors of opposite sign and actually, the hourly values may contain errors of up to 15K.

As shown in the previous sections, it is crucial to solve the problem of temperature and moisture profiles in order to accurately predict the cloud amount and the longwave fluxes. The error in temperature and moisture may arise from an incorrect prediction of the advection and moisture by the ECMWF model.

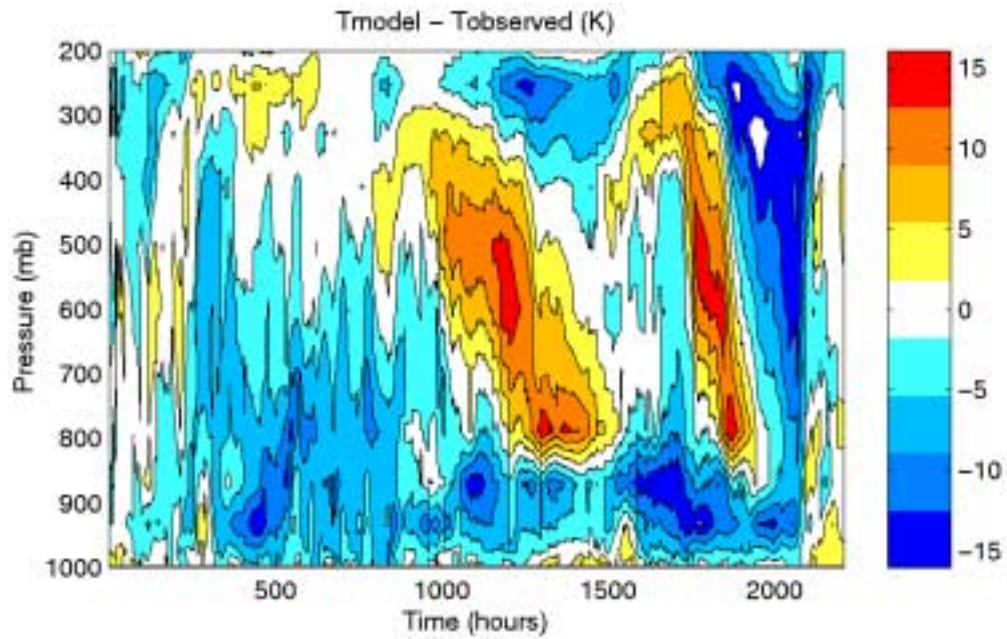


Figure 15: Temporal evolution of the error in temperature.
The simulated temperature is obtained with the 2D forcing.

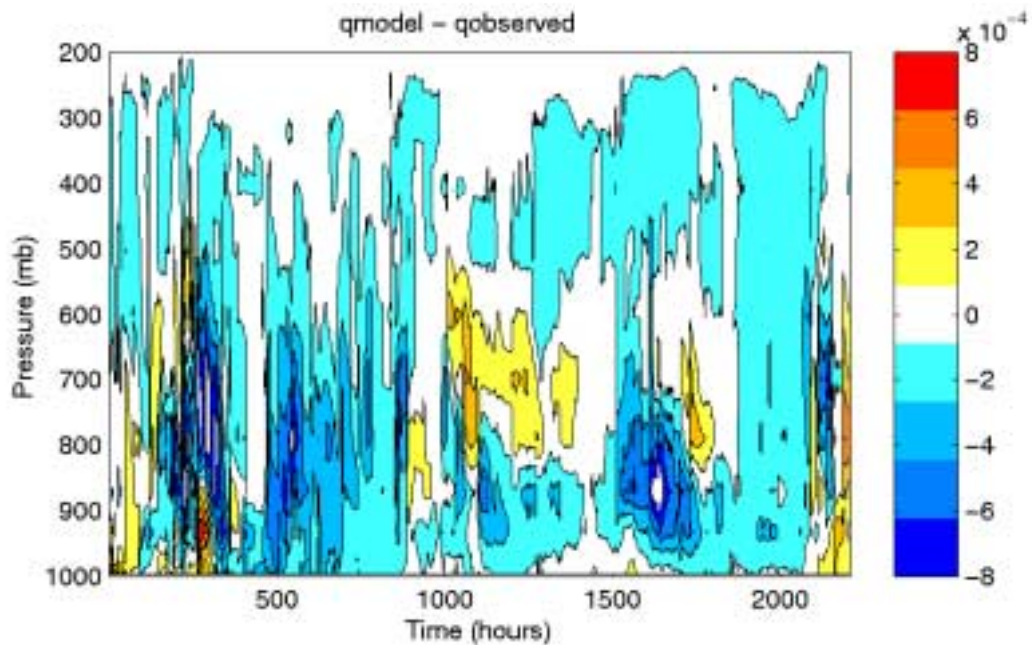


Figure 16: Temporal evolution of the error in moisture
The simulated moisture is obtained with the 2D forcing.

3.1.4 Surface fields

The surface fields include the surface temperature and turbulent heat fluxes of heat and moisture and they affect the properties of the boundary layer. The surface fields are either computed by the SCCM (*2D* and *3D* experiments) or prescribed from the observations (*sfc* and *relax* experiments). Time series of the modeled and the observed surface fields are shown in Figure 17 and mean values are given in Table 3. The time series in Figure 17 correspond to the *2D* forcing, and the *3D* forcing yields typically similar results. The model overestimates the surface temperature especially during the clear skies periods. The mean error is as much as 5 K for the whole winter. Moreover, the surface temperature is strongly damped in the model, suggesting a problem in the model surface energy budget. A possible source of error is that the SCCM treats the sea ice as an isothermal slab of 2 meters, but the sea ice does not respond at all like an isothermal slab. Beesley *et al.* (2000) encountered similar errors with the surface temperature in the ECMWF reanalysis.

The turbulent heat fluxes are computed through the use of bulk aerodynamics formulas (Kiehl *et al.*, 1996). The turbulent fluxes are positive upwards: for example, a positive value of the sensible heat fluxes means that the atmosphere is colder than the surface and receives heat from the surface. The average sensible heat flux is -2 W/m^2 and does not agree well with the observed average of -5 W/m^2 . On an hourly timescale, the differences between model and observations are striking. The discrepancies between modeled and observed latent fluxes are very large. The mean value modeled of the latent heat flux (11 W/m^2) differs from the observed mean value (0.1 W/m^2) by more than an order of magnitude for the winter period. These large biases in sensible and latent heat fluxes reveal a problem in the parameterization of the surface exchange. They are due to the combination of an overestimate of the surface mean wind and of errors in the gradients of temperature and specific humidity.

In order to test the cloud parameterization without the errors introduced by the surface exchange formulation, we prescribe the surface fields from the observations, as it is done in the *sfc* and *relax* forcing experiments.

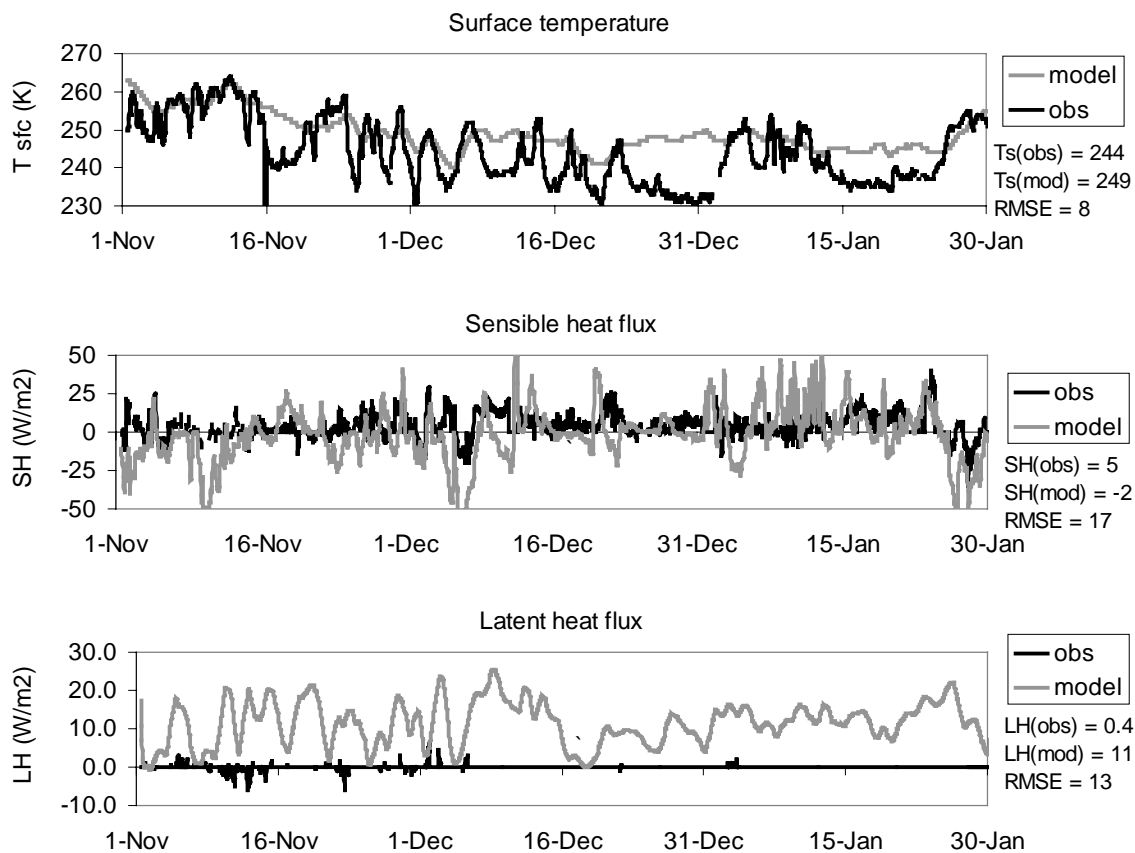


Figure 17: Time series of modeled surface temperature, sensible heat and latent heat fluxes. The modeled values are in gray and the observations are in black (Bretherton et al., 2001, Persson et al., 2001).

3. 2. Sensitivity to physical parameters and advective forcing

Several simulations have been conducted to investigate the cloud parameterization over the Arctic in CCM3 and the sensitivity to advective forcing. Each simulation is identical to the standard runs except for the changes made to the particular parameter, which is being tested. We have evaluated the influence of cloud type, and in particular of convective clouds (*C1*) and stratus associated to low-level inversions (*C3*). We have also evaluated the impact of the cloud microphysics itself i.e. the fraction of liquid in cloud condensate and the effective radius of ice droplets. We test the sensitivity of the simulations to errors in the specified advection of *T* and *q*.

3.2.1 Influence of cloud type

Three types of clouds are diagnosed by the SCCM: convective (*C1*), layered (*C2*) and stratus associated low-level inversions of temperature and moisture (*C3*). This parameterization is based on the type of clouds common at lower latitudes (Slingo, 1987). Over the Arctic, convective clouds are not common during wintertime. Moreover, the parameterization of clouds associated with low-level inversions is better suited for subtropical latitudes and does not represent well the Arctic clouds. It is important to understand the influence of the parameterization of these types of clouds (*C1* and *C3*) on wintertime simulations of the Arctic.

To determine the importance of convection in the simulations, the SCCM was integrated with the parameterization for convective clouds turned off (*C1 off*). The results of this run and the standard simulations are identical. This indicates that convection is negligible.

Secondly, we examine the impact of *C3* clouds on the simulations. Figure 18 compares the cloud fraction for standard experiments (*sdt*) with the experiment when the clouds associated with low-level inversions are turned off (*C3 off*) and Figure 19 shows the RMS errors of cloud fraction. In the *non-relax* simulations, turning off the *C3* clouds results in a better simulations: the

time series of cloud fraction improves and the RMSE is lower. In the *relax* simulations, turning off C3 clouds does not change significantly the cloud amount and the RMSE. In the standard experiment, the SCCM produces few C3 clouds with the *relax* forcing and more C3 clouds with the *non-relax* forcing (2D, 3D and *sfc*). So, turning off C3 clouds does not have a significant impact with *relax* forcing but it has a larger effect with *non-relax* forcing.

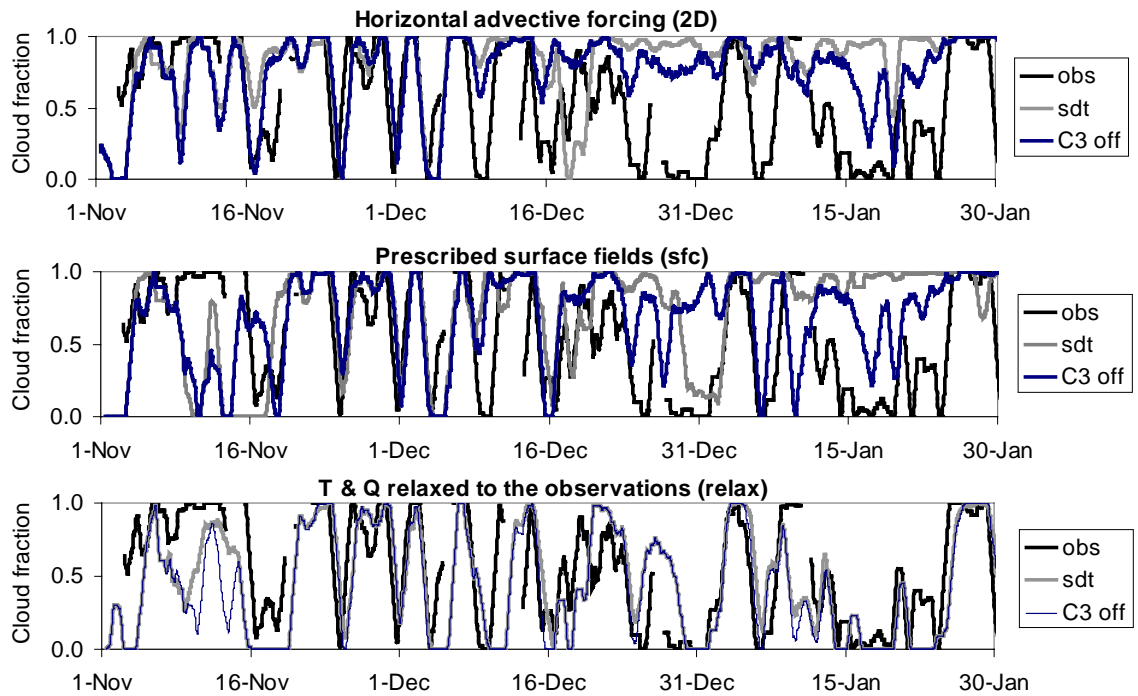


Figure 18: Impact of C3 clouds on the cloud fraction.

The standard simulation (*sdt*) is shown in gray and C3 off in blue and the observations in black.

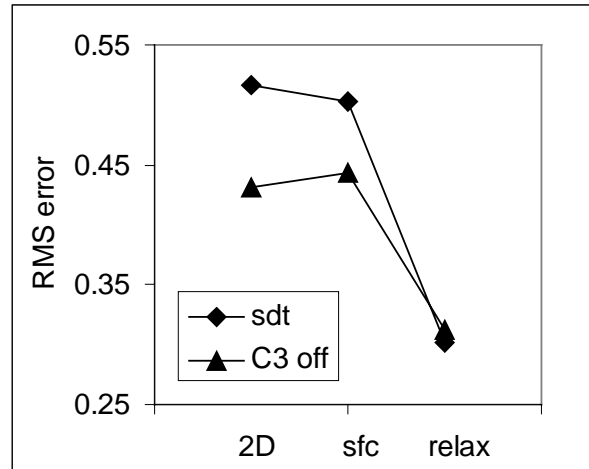


Figure 19: Impact of C3 clouds on the RMS error of the cloud fraction.
 The standard simulation (sdt) is shown by the solid triangle and C3 off by the solid diamond

Turning off C3 clouds has different impact with the *non-relax* forcing (2D, 3D and *sfc*) than with the *relax* forcing. This difference is likely correlated to the bias of the temperature and moisture inversion profiles in the *non-relax* experiments. The C3 clouds are strongly linked to the boundary layer and are associated with low-level inversions in temperature and moisture. More exactly, the SCCM diagnoses C3 clouds if the lapse rate in the most stable layer reaches a threshold value of -0.125 K/mb. This means that an inaccurate representation of the inversion has an influence on the amount of C3 clouds produced by the model and, in turn, this has in turn an influence on the cloud fraction. Figure 20 illustrates how an error in the lapse rate affects the cloud amount. We assume a relative humidity of 0.8 and we compute the cloud fraction for three lapse rates. The cloud amount is 0.0, 0.2 and 1.0 if the lapse rate is respectively 0.1 C/mb (no inversion), -0.2 C/mb (weaker inversion) or -0.5 C/mb (stronger inversion).

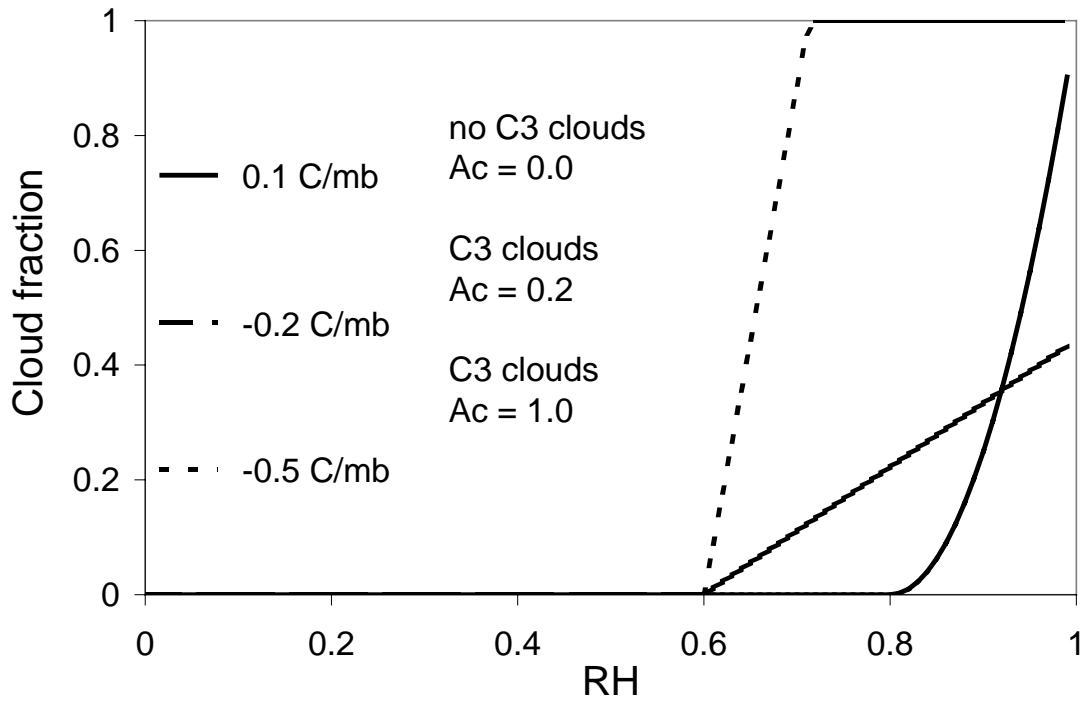


Figure 20: Impact of the inversion strengths on the cloud fraction. The relative humidity is set to 0.8. For lapse rates equal to 0.1 C/mb, -0.2 C/mb and -0.5 C/mb, the cloud fraction is 0.0, 0.2 and 1.0 respectively.

In conclusion, turning off the C3 clouds improves the simulations with *2D* and *sfc* forcing. However, the cloud fraction is still overestimated compared with the *relax* forcing. Turning off the C3 clouds does not solve all the problem with the cloud fraction and it is still very important getting accurate T and q profiles.

3.2.2 Influence of the ice effective radius

The microphysical properties of clouds strongly influence their radiative properties. Factors such as hydrometeor size and distribution of water in the cloud determine how clouds affect

radiative heating profiles in the atmosphere (Curry *et al.*, 1992). The impact of effective radius on simulation is discussed in this section, and the influence of ice liquid ratio in the clouds is discussed in the subsequent section.

In the standard simulations, the SCCM sets the effective radius of liquid and ice droplets to 10 μm , over the oceans. Notice that in the standard CCM3 parameterization package, the ice effective radius is also dependent on the normalized pressure and it increases from 10 to 30 μm with height (see Appendix A: Cloud parameterization). The increase in ice effective radius with height is a parameterization based on what is occurring at lower latitudes where one can expect liquid clouds at lower altitudes and an increase in ice amounts with height. As a result, one might expect ice effective radius to also increase with height. However, this is not a good assumption for layered clouds in the arctic, therefore in these simulations, the ice effective radius was kept constant with height.

Shupe *et al.* (2001) found from radar and radiometer measurements that during April-July time period during the SHEBA experiment, the liquid effective radius ranges from 3 to 20 μm with a mean value of 7 μm , and the ice effective ranges radius from 7 to 300 μm with a mean value of 60 μm . The SCCM parameterization has a good approximation of the liquid hydrometeor sizes but it underestimates the ice size, at least, during summer and this is also likely true during winter. One may argue that the extrapolation of summer ice effective radius to winter is somewhat delicate. During the observation's period (April-July), low-level clouds are typically in mixed-phase (Shupe *et al.*, 2001). The monthly-averaged percentages of clouds with liquid varies between 70 and 93% (Intrieri *et al.*, 2001b). This means that there is significant liquid water present, and therefore, there is a large supply of water for ice crystals to grow on and the ice effective radius is large. During the simulations' period (November-January), the observed monthly-averaged percentages of clouds with liquid is only 25% to 65% (Intrieri *et al.*, 2001b). The water contents are lower so the ice sizes are probably smaller during winter. However, the summer values give an estimate of the maximum ice effective radius range and we use these values for our wintertime simulations. The ice effective radius was set successively to 10, 50, 100, 200 and 300 μm .

If the SCCM underestimates the ice effective radius, therefore, it may overestimate the downwelling longwave flux. For a given cloud water content, the LW radiation can more easily penetrate a cloud composed of a few big droplets than one containing many small droplets. As a result, an increase in the droplets size for a given water content, increases the amount of longwave radiation lost to space and decreases the downwelling LW flux. This appears to be the case in the simulations: increases in the ice effective radius result in decreases in the downwelling fluxes (Figure 21).

In the cloud parameterization, the cloud fraction is not directly dependent on the ice effective radius. However, one may expect that as increasing ice effective radius modifies the LW flux, it will in turn change the temperature profiles and consequently, the cloud fraction. However, as Figure 22 shows, this is not the case in these sensitivity tests.

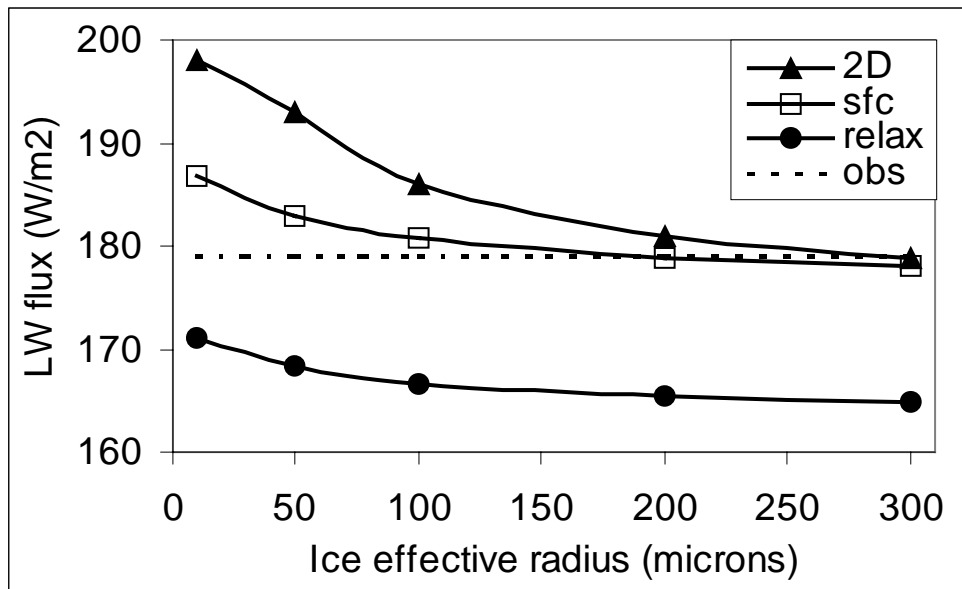


Figure 21: Impact of ice effective radius on downwelling LW flux. The ice effective radius varies between 10 μm to 300 μm . The downwelling LW fluxes correspond to the winter average (November-January). The observed LW fluxes (dashed line) are compared to the simulated (2D, sfc and relax) LW fluxes (solid lines).

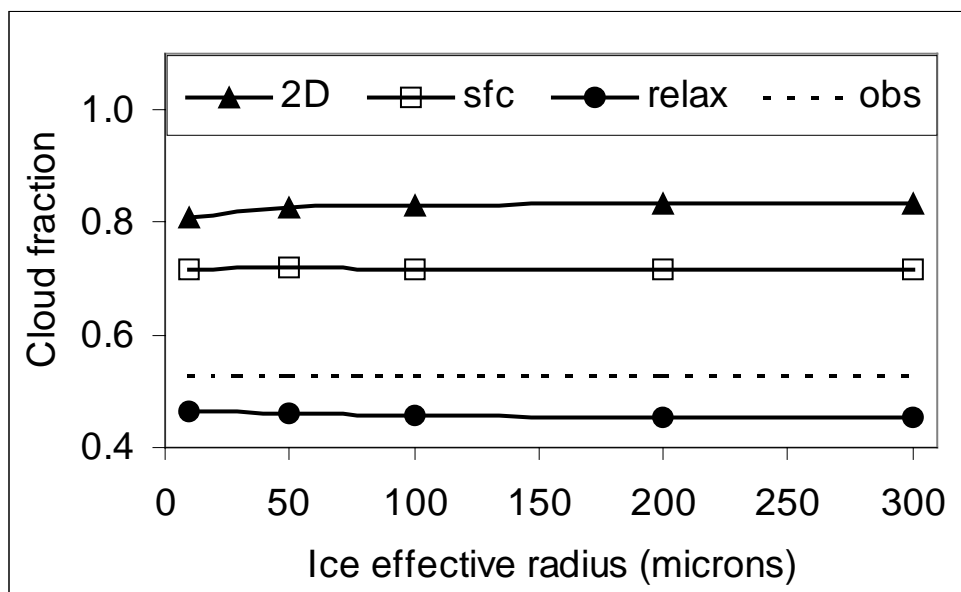


Figure 22: Impact of ice effective radius on cloud fraction. The cloud fraction is averaged over the winter (November-January). The observed low level cloud amount (dashed line) is compared to the simulated (2D, sfc and relax) cloud amount (solid lines) for ice effective radius ranging from 10 μm to 300 μm .

3.2.3 Influence of the ice liquid ratio

As explained above, the model initiates ice clouds below -10 C and turns off the liquid phase below -30 C. Lidar and radar observations during the SHEBA experiment have shown that Arctic clouds may contain ice at temperatures above -10 C and supercooled water may be present up to -34 C (Intrieri *et al.*, 2001b, Bretherton *et al.*, 2001). We have performed simulations using the fraction of liquid taken from the observations (see dashed line in Figure 23) instead of the original parameterization. Using the more realistic liquid water fraction has a minor impact on the simulations.

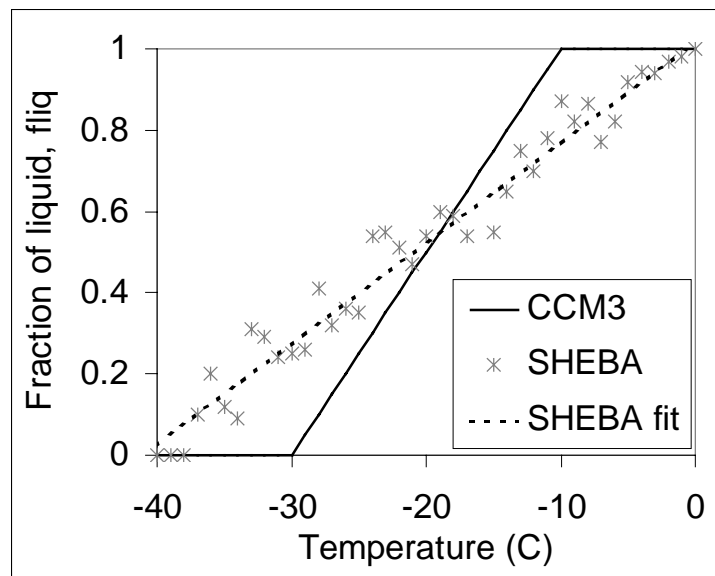


Figure 23: Fraction of liquid phase in clouds.

The parameterized liquid fraction of the cloud condensate (solid line) is compared to the lidar observations at SHEBA (asterisk). The dashed line is a linear fit of the lidar observations.

3.2.4 Impact of forcing uncertainty

The SCCM requires values for the advection of temperature and moisture and as discussed earlier, these values are prescribed from the ECMWF reanalysis. As stressed in section 2. 1., these tendencies need to be accurate in order to prevent an accumulation of errors. Bretherton *et al.* (2001) have discussed the validity of the ECMWF tendencies of temperature and moisture and they deduced that these mean tendencies appear accurate on a monthly time scale. However, the hourly values that are used in our simulations could be imprecise and it is important to have an idea of the sensitivity of the simulations in the uncertainty of the advective forcing.

We have performed simulations where the advective forcing of both T and q has been increased and decreased by 20 %. It is a crude way to vary thermodynamics profiles but we do not attempt to improve simulations of T and q but to check on the sensitivity to advective forcing. Figure 24 shows the RMS errors for the simulations integrated with 2D forcing. The best simulations of T and q profiles within the column are obtained with the *sdt* forcing. The ECMWF model is forced with observed T and q and computes the advection of T and q to be consistent with the observed T and q. It is why we obtain the best results for T and q profiles with the standard advection. The best results in downwelling LW flux and surface temperature are obtained when the advective forcing is reduced from 20%. Beesley *et al.* (2000) has observed large differences in the surface temperature between ECMWF model and observations. The ECMWF computes the advection and T and q to be consistent with the computed surface temperature and not with the observations. The advection of T and q contains likely larger errors near the surface and it is why the best results are obtained when the advection is reduced. The cloud fraction is not very sensitive to changes in the advective tendencies.

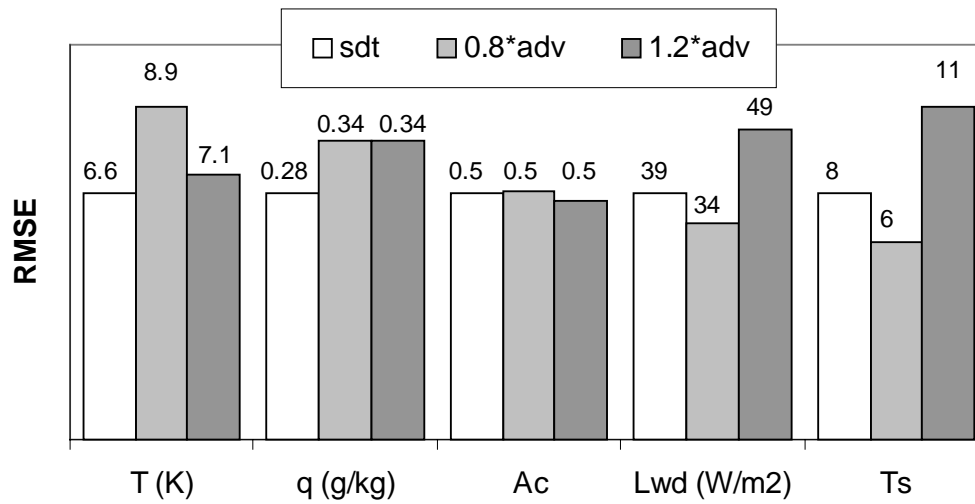


Figure 24: Sensitivity to advective forcing

The RMS error of the T profile (T), q profile (q), cloud fraction (Ac), downwelling LW flux (LWd) and surface temperature (Ts) are integrated with 2D forcing. The standard experiment is in white and the 20-percent-decrease in advection in light gray and the 20-percent-decrease in dark gray.

CHAPTER 4 - CONCLUSION

This research has been motivated by the fact that CCM3 significantly overestimates the cloud amount in the Arctic during the wintertime, when compared to the observations. Our goal is to understand the deficiencies in CCM3 that lead to these errors in Arctic cloudiness during winter and how modifications of the cloud parameterization could improve the simulations.

The SCCM (the column version of CCM3) is used to evaluate the cloud parameterization of CCM3. The model is initialized and forced with a data set constructed from SHEBA observations and ECMWF reanalysis. We have performed two sets of experiments: the first set was integrated with the standard package of parameterizations of CCM3 and the second set was a suite of sensitivity studies of cloud parameterization and advective forcing uncertainty.

In the standard experiments, we have explored several approaches of prescribing observed forcing, and in each case, we examine the issues of the column model in reproducing Arctic clouds and radiative fluxes. Our main results for the standard simulations were:

- When the forcing terms include only large-scale advection of temperature and moisture and vertical velocity, the SCCM overestimates the cloud amount and the downwelling LW fluxes. Moreover, the model does not capture accurately the temperature and moisture profiles, and the surface flux fields. In the low-level cloud layers, the modeled atmosphere is too warm and too dry compared to observations. The modeled mean surface temperature is overestimated and the variability is damped when compared to the observations. The turbulent surface fluxes are poorly represented, especially the latent heat fluxes that differs from observations by more than an order of magnitude.
- Prescribing the surface fields from observations slightly improves the simulations. However, cloud amounts are still too large and downwelling LW fluxes are too small.
- Relaxing the T and q profiles to observed values dramatically improves the simulations. Clouds and LW fluxes are reproduced fairly well on a monthly as well as on the daily

timescale. This suggests that the cloud parameterization of CCM3 is suitable for Arctic clouds, as long as the temperature and moisture fields are correctly captured.

Sensitivity studies investigate the influence of cloud type, ice effective radius and ice liquid ratio amount. The main results are:

- Convective clouds do not occur in the simulations, as one expects during Arctic winter, since there is no surface heating by the sun.
- Clouds associated with low-level inversions of the lapse rate (C3) occur more frequently when T and q are calculated by the SCCM than when T and q are prescribed from the observations. Turning off the C3 clouds slightly improves the simulations with *2D* and *sfc* forcings, as seen in reduced RMS error.
- The ice effective radius is underestimated in the model compared to the observations. Increasing the ice effective radius decreases the downwelling LW fluxes but the cloud fraction is not very sensitive to an increase in ice particle size.
- Prescribing the ice liquid ratio in cloud water from the observation has a minimal impact on the simulations of cloud fraction.
- The cloud fraction is not very sensitive to the 20-percent changes in T and q advection forcings.

Our study allows us to understand better why the CCM3 overestimates the Arctic cloud fraction during the wintertime. The CCM3 cloud parameterization works moderately well over the Arctic if the thermodynamic profiles are accurate. More accurate reproductions of temperature and moisture fields will likely result from changes in the boundary layer parameterization. Our results also suggest that improvements are necessary in the surface flux parameterization.

APPENDIX A: CLOUD PARAMETERIZATION

The cloud fraction is evaluated via a diagnostic method, which is a generalization of Slingo's scheme (Slingo, 1987). Cloud fraction depends on relative humidity, vertical velocity, atmospheric stability and convective mass flux associated with parameterized moist convection. Three types of cloud are diagnosed from the scheme: convective cloud, layered cloud and low-level marine stratus.

The *total column convective cloud amount* is diagnosed from the presence and the strength of moist convective activity. It is a function of the averaged moist convective mass flux, $\overline{M_c}$ diagnosed by the moist convective parameterization.

$$\overline{A_{conv}} = 0.035 \ln(1 + \overline{M_c}) \quad (14)$$

The large-scale relative humidity is adjusted to take into account the assumption that the fraction of convective cloud, $\overline{A_{conv}}$ is saturated.

$$RH' = \frac{RH - A_{conv}}{1 - A_{conv}} \quad (15)$$

The remaining cloud types are diagnosed on the basis of RH' . *Frontal and tropical low cloud fraction* (i.e. the clouds occurring below 750 mb) are diagnosed according to:

$$A_c = \begin{cases} 0 & \omega > \omega_c \\ \left(\frac{\omega_c - \omega}{\omega_c} \right) \left(\frac{RH' - RH_{min}^{low}}{1 - RH_{min}^{low}} \right)^2 & 0 \leq \omega \leq \omega_c \\ \left(\frac{RH' - RH_{min}^{low}}{1 - RH_{min}^{low}} \right)^2 & \omega < 0 \end{cases} \quad (16)$$

The low level cloud fraction associated with low-level inversions is determined from:

$$A_c = \begin{cases} 0 & RH' < 0.6 \\ -6.67 \left(\frac{\partial \theta}{\partial p} - 0.1 \right) \left(\frac{RH' - 0.6}{0.3} \right) \left(\frac{P - 750}{150} \right) & 0.6 \leq RH' \leq 0.9 \\ -6.67 \left(\frac{\partial \theta}{\partial p} - 0.1 \right) \left(\frac{P - 750}{150} \right) & RH' > 0.9 \end{cases} \quad (17)$$

where $\frac{\partial \theta}{\partial p}$ is the maximum inversion strength. The pressure factor $\left(\frac{P - 750}{150} \right)$ accounts for the transition for marine stratus clouds that occur in the presence of low-level inversions. The parameter set to 50 mb/day allows low-level clouds to form under weak subsidence conditions. The parameter RH_{min}^{low} is set to 0.9 over open ocean and 0.8 over land.

Middle and upper level cloud fractions (i.e. the clouds occurring above 750 mb) are deduced from the relation:

$$A_c = \left[\max \left(0, \frac{RH' - RH_{lim}}{1 - RH_{lim}} \right) \right]^2 \quad (18)$$

where RH_{lim} is a function of the Brunt-Vaisalla frequency.

The optical cloud properties are accounted for, using the Slingo parameterization Slingo, 1989. In this scheme, the cloud water path and the effective radius are used to determine the solar radiative properties of clouds Lee *et al.*, 1997. The cloud water path (CWP) is diagnosed as a function of the water vapor relative humidity. The cloud water path is the cloud water mass integrated vertically over the cloud and it may be interpreted as the cloud thickness. The effective radius, r_e may be seen as a measure of the mean droplet size weighted by the droplet cross section. CCM3 differentiates the effective radius over maritime and continental regions. Over the ocean, the effective radius of a cloud droplet is set to 10 μm . Over landmasses, the effective radius is dependent on temperature and it varies between 5 and 10 μm . Below -30C , CCM3 diagnoses an ice particle effective radius from the normalized pressure.

The fraction of cloud water in the form of liquid water or ice is diagnosed from the temperature.

$$f_{ice} = \begin{array}{ll} 0 & T > -10C \\ -0.05(T + 10) & -30C \leq T \leq -10C \\ 1 & T < -30C \end{array}$$

APPENDIX B: SYMBOL DEFINITION

In this appendix, we present a table containing the symbols used in this text and their meanings. In developing the symbols used in this book, we attempted to conciliate the respect of traditions in physical climatology with the coherence and simplicity of the text.

English symbols

A_c	Fractional area coverage by clouds
AMIP	Atmospheric Model Intercomparison Project
C_{LW}	Cloud radiative forcing in the longwave
C_{SW}	Cloud radiative forcing in the shortwave
C_{net}	Net cloud radiative forcing
C_p	Specific heat of air at constant pressure
$C1$	Convective cloud
$C2$	Layered cloud
$C3$	Cloud associated with low-level inversions
CCM	Climate Community Model
CCN	Cloud Condensei Nuclei
CSM	Climate System Model
CWP	Cloud Water Path
ECMWF	European Centre for Medium-Range Weather Forecasts
F_{LW}	Longwave radiative flux
F_{SW}	Shortwave radiative flux
GCM	Global Circulation Model

LH	Latent heat flux
LWd	Downwelling longwave radiative flux
LWu	Upwelling longwave radiative flux
NCAR	National Center for Atmospheric Research
p	Pressure
q	Moisture
q_{obs}	Observed moisture
R	Gas constant for air
<i>relax</i>	relaxation of T and q profile to the observations
RH	Relative humidity
RMSE	Root Mean Square Error
SCCM	Single-Column version of CCM3
SCM	Single Column Model
<i>sfc</i>	Prescribed surface conditions
SH	Sensible Heat Flux
SHEBA	Surface Heat Budget of the Arctic Ocean
T	Temperature
T_{obs}	Observed temperature
t	time
TOA	Top of the Atmosphere
V	Horizontal velocity

Greek symbols

τ Relaxation timescale

ω Vertical velocity

Miscellaneous symbols

2D Horizontal advective forcing

3D Revealed forcing

REFERENCES

- Beesley, J. A. and Moritz, R. E., 1999: Toward an Explanation of the Annual Cycle of Cloudiness over the Arctic Ocean. *J. Clim.*, **12**, 395-415.
- Beesley, T. A., Bretherton, C. S., Jakob, C., Andreas, E. L., Intrieri, J. M. and Uttal, T. A., 2000: A comparison of the ECMWF forecast model with observations at SHEBA. *J. Geophys. Res.*, **105**, 12,337-12,349.
- Betts, A. K. and Miller, M. J., 1986: A new convective adjustment scheme. Part II: Single Column tests using GATE wave, BOMEX, ATEX, and arctic air-mass data sets. *Quart. J. Roy. Meteor. Soc.*, **112**, 693-709.
- Bretherton, C. S., de Roode, S. R. and Jakob, C., 2001: A comparison of the ECMWF forecast model with observations over the annual cycle at SHEBA. *Submitted to J. Geophys. Res.*,
- Clark, M. P., Serreze, M. C. and Barry, R. G., 1996: Characteristics of Arctic Ocean climate based on COADS data, 1980-1993. *Geophys. Res. Lett.*, **23**, 1953-1956.
- Curry, J. A. and Ebert, E. E., 1992: Annual cycle of radiation fluxes over the Arctic Ocean: Sensitivity to cloud optical properties. *J. Clim.*, **5**, 1267-1280.
- Curry, J. A., Rossow, W. B., Randall, D. and Schramm, J. L., 1996: Overview of Arctic Cloud and Radiation Characteristics. *J. Clim.*, **9**, 1731-1764.
- ECMWF Research Department, 1988: ECMWF forecast model, adiabatic part (2nd edition). *European Centre for Medium Range Weather Forecasts and E. Reading*,
- ECMWF Research Department, 1991: ECMWF forecast model, physical parameterisation (3rd edition). *R. European Centre for Medium Range Weather Forecasts, England.*,
- Hack, J. J. and Pedretti, J. A., 2000: Assessment of Solution Uncertainties in Single-Column Modeling Frameworks. *J. Clim.*, **13**, 352-365.
- Hack, J. J., Pedretti, J. A. and Petch, J. C., 1999: SCCM User's Guide. *Website*, <http://www.cgd.ucar.edu:80/cms/sccm/userguide.html#1>.

- Hahn, C. J., Warren, S. G. and London, J., 1995: The Effect of Moonlight on Observatin of cloud Cover at Night, and Application to Cloud Climatology. *J. Clim.*, **8**, 1429-1446.
- Intrieri, J. M., Fairall, C. W., Shupe, M. D., Persson, P. O. G., Andreas, E. L., Guest, P. S. and Moritz, R. E., 2001a: An annual cycle of Arctic surface cloud forcing at SHEBA. *Submitted to J. Geophys. Res.*,
- Intrieri, J. M., Shupe, M., Mc Carty, B. J. and Uttal, T. A., 2001b: Annual cycle of arctic cloud statistics from lidar and radar at SHEBA. *Submitted to J. Geophys. Res.*,
- Key, J., Slayback, D., Xu, C. and Schweiger, A., 1999: New climatologies of polar clouds and radiation based on the ISCCP "D" products. *Proceedings of the 5th conference on polar meteorology. 10-15 January 1999, Dallas, Texas.*,
- Kiehl, J. T., Hack, J. J., Bonan, G. B., Boville, B. A., Briegleb, B. P., Williamson, D. L. and Rasch, P. J., 1996: Description of the NCAR Community Climate Model (CCM3). *National Center for Atmospheric Research*, 152 pp.
- Lee, W.-L., Iacobellis, S. F. and Somerville, R. C., 1997: Cloud Radiation Forcings and Feedbacks: General Circulation Model Tests and Observational Validation. *J. Clim.*, **10**, 2479-2496.
- Liou, K., 1992: Radiation and Cloud Processes in the Atmosphere. *O. P. University*, New-York
- Makshtas, A. P., Andreas, E. L., Svyashchennikov, P. N. and Timachev, V. F., 1999: Accounting for clouds in sea-ice models. *Atmos. Res.*, **52**, 77-113.
- Minnis, P., Doelling, D. R., Uttal, T. A., Arduini, R. F. and Shupe, M., 2001: Cloud coverage during FIRE ACE derived from AVHRR data. *Submitted to J. Geophys. Res.*,
- Nemesure, S., Cess, R. D. and Dutton, E. G., 1994: Impact of Clouds system of snow-covered surfaces. *J. Clim.*, **7**, 579-585.
- Perovich, D. K., Andreas, E. L., Fairall, C. W., Guest, P. S., Persson, P. O. G. and others., a., 1999: Year on ice gives climate insights. *EOS, Transactions, AGU*, **41**, 481-486.
- Persson, P. O. G., Fairall, C. W., Andreas, E. L. and Guest, P. S., 2001: Measurements of the meteorological conditions and surface energy budget near the atmospheric surface flux group tower at SHEBA. *Submitted to J. Geophys. Res.*,

- Pinto, J. O., Curry, J., Lynch, A. H. and Persson, P. O. G., 1999: Modeling clouds and radiation for the November 1997 period of SHEBA using a column climate model. *J. Geophys. Res.*, **14**, 6661-6678.
- Ramanathan, V., Cess, R. D., Harrison, E. F., Minnis, P., Barkstrom, B. R., Ahmad, E. and Hartman, D., 1989: Cloud-radiative forcing and climate: Results from the Earth Radiation Budget Experiment. *Science*, **243**, 57-63.
- Randall, D., Xu, K.-M., Somerville, R. C. and Iacobellis, S. F., 1996: Single-Column Models and Cloud Ensemble Models as Links between Observations and Climate Models. *J. Clim.*, **9**, 1683-1697.
- Randall, D. A. and Cripe, D. G., 1999: Alternative methods for specification of observed forcing in single-column models and cloud system models. *J. Geophys. Res.*, **104**, 24,527-24,545.
- Shupe, M. D., Uttal, T., Matrosov, S. Y. and Shelby, F. A., 2001: Cloud Water Contents and Hydrometeor Sizes During the FIRE-Arctic Clouds Experiment. *Submitted to J. Geophys. Res., FIRE-ACE, Special Issue*,
- Slingo, A., 1989: A GCM parameterization for the shortwave radiative properties of water clouds. *J. Atmos. Sci.*, **46**, 1419-1427.
- Slingo, J. M., 1987: The development and verification of a cloud prediction scheme for the ECMWF model. *Quart. J. Roy. Meteor. Soc.*, **113**, 899-927.
- Tao, X., Walsh, J. and Chapman, W. L., 1996: An assessment of global climate model simulations of Arctic air temperatures. *J. Clim.*, **9**, 1060-1076.
- Walsh, J. E. and Chapman, W. L., 1998: Arctic cloud-radiation-temperature associations in observational data and atmospheric reanalysis. *J. Clim.*, **11**, 3030-3045.